

Cytoarchitecture of the human lateral occipital cortex: mapping of two extrastriate areas hOc4la and hOc4lp

Aleksandar Malikovic · Katrin Amunts · Axel Schleicher · Hartmut Mohlberg · Milenko Kujovic · Nicola Palomero-Gallagher · Simon B. Eickhoff · Karl Zilles

Received: 5 November 2014 / Accepted: 9 February 2015 / Published online: 17 February 2015
© Springer-Verlag Berlin Heidelberg 2015

Abstract The microstructural correlates of the functional segregation of the human lateral occipital cortex are largely unknown. Therefore, we analyzed the cytoarchitecture of this region in ten human post-mortem brains using an observer-independent and statistically testable parcellation method to define the position and extent of areas in the lateral occipital cortex. Two new cytoarchitectonic areas were found: an anterior area hOc4la and a posterior area hOc4lp. hOc4la was located behind the anterior occipital sulcus in rostral and ventral portions of this region where it occupies the anterior third of the middle and inferior lateral occipital gyri. hOc4lp was found in caudal and dorsal

portions of this region where it extends along the superior and middle lateral occipital gyri. The cytoarchitectonic areas were registered to 3D reconstructions of the corresponding brains, which were subsequently spatially normalized to the Montreal Neurological Institute reference space. Continuous probabilistic maps of both areas based on the analysis of ten brains were generated to characterize their inter-subject variability in location and size. The maps of hOc4la and hOc4lp were then used as seeds for meta-analytic connectivity modeling and quantitative functional decoding to identify their co-activation patterns and assignment to functional domains. Convergent evidence from their location, topography, size, functional domains and connectivity indicates that hOc4la and hOc4lp are the potential anatomical correlates of the functionally defined lateral occipital areas LO-1 and LO-2.

Keywords Human visual cortex · Cytoarchitecture · Lateral occipital cortex · Probabilistic maps · Brain mapping · Functional meta-analysis · LO-1 · LO-2

A. Malikovic · K. Amunts · A. Schleicher · M. Kujovic
C. and O. Vogt Institute for Brain Research, Heinrich Heine
University, 40225 Düsseldorf, Germany

A. Malikovic · K. Amunts · H. Mohlberg ·
N. Palomero-Gallagher · S. B. Eickhoff · K. Zilles
Institute of Neuroscience and Medicine (INM-1), Research
Centre Jülich, 52425 Jülich, Germany
e-mail: k.zilles@fz-juelich.de

A. Malikovic (✉)
Institute of Anatomy, Faculty of Medicine, University of
Belgrade, Dr Subotica 4/II, 11000 Belgrade, Republic of Serbia
e-mail: aleksa-m@eunet.rs

S. B. Eickhoff
Institute of Clinical Neuroscience and Medical Psychology,
Heinrich Heine University, 40225 Düsseldorf, Germany

K. Zilles
Department of Psychiatry, Psychotherapy and Psychosomatics,
RWTH Aachen University, 52062 Aachen, Germany

K. Zilles
JARA-Brain, Jülich-Aachen Research Alliance, 52428 Jülich,
Germany

Introduction

The human lateral occipital cortex represents a broad region interposed between visual area V5/MT located anteriorly, and visual areas V3 (V3d and V3v) and V3A both located posteriorly. Functional imaging studies demonstrated that this region is involved in visual object perception and visual motion processing. Rostral and ventral parts of this region are functionally defined as lateral occipital complex (LO or LOC), that responds preferentially to images of objects, independent of the particular image features that define the object shape (e.g., luminance, contrast, motion and texture) (Grill-Spector et al. 2001;

Kourtzi and Kanwisher 2001; Larsson and Heeger 2006; Malach et al. 1995; Sarkheil et al. 2008; Vinberg and Grill-Spector 2008). Furthermore, LOC may be subdivided by its responses to the location and size of objects (Grill-Spector et al. 1999; Sawamura et al. 2005), to differences in perceived 3D object shape (Kourtzi et al. 2003; Murray et al. 2003), to familiar objects and abstract 2D shapes (Stanley and Rubin 2005), and to intact images of common objects (Larsson and Heeger 2006). Caudal and dorsal parts of human LOC are specialized in the processing of kinetic contours (boundaries) that combine both shape and motion information (Dupont et al. 1997; Grossman et al. 2000; Kononen et al. 2003; Tootell and Hadjikhani 2001; Van Oostende et al. 1997) and respond to second-order motion (Smith et al. 1998). In the first case, this cortical region is referred as the kinetic occipital region (KO); while in the second case, it is indicated as a motion-sensitive area V3B. There are two alternative views related to the function of KO. According to the first view, KO is considered to be a region specialized in contour processing in general, rather than in specialized processing of kinetic contours that define the object shape (Zeki et al. 2003). According to the second view, KO represents the cortical region that includes multiple visual areas (V3, V3B, LO-1, LO-2), rather than a single entity specialized in the processing of kinetic contours (Larsson et al. 2010).

Retinotopic mapping of the human lateral occipital cortex is a highly successful approach to study its segregation (Sereno et al. 1995; Wandell et al. 2007). In the LOC, Smith et al. (1998) described a topographic representation of the lower quadrant of the contralateral visual field, area V3B, in a cortical region adjacent to visual area V3A. Later, both, the upper and lower quadrants of the visual field were identified in V3B (Press et al. 2001). Eccentricity-based mapping has shown that some regions within the LOC are more responsive to the fovea, while others are more responsive to the periphery of the visual field. Tootell and Hadjikhani (2001) subdivided the lateral occipital cortex into two regions representing the central (LOC) and peripheral (LOP) visual field, respectively. This was confirmed by Seiffert et al. (2003). The study of Larsson and Heeger (2006) demonstrated the existence of two separate topographic representations of the contralateral visual hemifield in LOC. They described a posterior (LO-1) and an anterior (LO-2) lateral occipital area in the human brain. Retinotopic representation in LO-1 was the mirror of that in V3, while that in LO-2 was the mirror of that in LO-1. The borders between these areas represent the lower (V3/LO-1) and upper (LO-1/LO-2) vertical meridian. These and the studies of Swisher et al. (2007), Wandell et al. (2007), Kolster et al. (2010) and Henriksson et al. (2012) have established LO-1 and LO-2 as distinct, functionally defined areas within the higher lateral

extrastriate human visual cortex. Furthermore, recent studies have demonstrated functional differences between LO-1 and LO-2. LO-2 but not LO-1 contains object-selective representations (Sayres and Grill-Spector 2008), and LO-2 but not LO-1 overlaps with body part-selective regions (Weiner and Grill-Spector 2011). Comparisons between functional maps and myelin-based contrast detected by MRI indicated a close relation between functional and structural partitioning in many regions of the visual cortex, but also some interesting differences, which require further evaluations of both approaches (Abdollahi et al. 2014; Glasser and Van Essen 2011; Glasser et al. 2014).

The functional specialization and distinct retinotopic organization of the human LOC provide strong evidence for a cytoarchitectonic segregation of this region. To test this hypothesis, we analyzed the cytoarchitecture of the LOC region in 10 human post-mortem brains using an observer-independent parcellation method (Schleicher et al. 1999, 2000, 2005). We found two distinct lateral occipital cytoarchitectonic areas: an anterior (hOc4la) and a posterior (hOc4lp) area. We defined their borders, extents, relationships to the occipital sulci and gyri, volumes and stereotaxic locations. Furthermore, principal component and hierarchical cluster analyses suggest a hierarchically high position of both areas together with the fusiform areas FG1 and FG2 and a position between the dorsal and ventral visual streams. Subsequently, we performed meta-analytic connectivity modeling as well as quantitative functional decoding of both regions to identify functional correlates of hOc4la and hOc4lp.

Materials and methods

Post-mortem sample and histological processing

Cytoarchitectonic analysis of the LOC was performed in 10 human post-mortem brains (5 male and 5 female; mean age 66.3 years, age range 37–85 years; post-mortem delay less than 24 h; Table 1). The brains were obtained from the body donor program of the Institute of Anatomy, University of Düsseldorf, Germany from subjects with no clinical history of neurological or psychiatric diseases, with the exception of brain number 3, which came from a subject with a transitory motor impairment. The same post-mortem sample was analyzed in previous cytoarchitectonic studies of visual areas (Amunts et al. 2000; Caspers et al. 2013; Kujovic et al. 2013; Malikovic et al. 2007; Rottschy et al. 2007).

The brains were removed from the skull and fixed for several months in either 4 % formalin or Bodian's fixative. During fixation, the brains were suspended on the vertebral arteries in the fixative solution to avoid

Table 1 Brains used for cytoarchitectonic mapping of the lateral occipital cortex

Brain	Age (years)	Gender	Cause of death	Post-mortem delay (h)	Weight prior to fixation (g)	Fixation fluid
1	79	Female	Bladder carcinoma	24	1350	Bodian
2	56	Male	Rectal carcinoma	24	1270	Formalin
3	69	Male	Cardiovascular disease	16	1360	Formalin
4	75	Male	Acute glomerulonephritis	24	1349	Formalin
5	59	Female	Cardiorespiratory insufficiency	24	1142	Formalin
6	54	Male	Myocardial infarction	8	1622	Formalin
7	37	Male	Cardiac arrest	24	1437	Formalin
8	72	Female	Renal failure	12	1216	Formalin
9	79	Female	Cardiorespiratory insufficiency	16	1110	Bodian
10	85	Female	Mesenteric artery infarction	14	1046	Bodian

compression or major distortions. After fixation and prior to embedding and sectioning, MR imaging of each post-mortem brain was performed using a Siemens 1.5 T Magnetron scanner (Erlangen, Germany) with T1-weighted 3D FLASH sequence (flip angle 40°, repetition time TR = 40 ms, echo time TE = 5 ms). This procedure provided a reference data set to correct the distortions of brain shape and size that inevitably occur during histological processing.

After MR imaging, the brains were dehydrated in a graded series of increasing ethanol concentration, embedded in paraffin, and continuous serial whole brain sections (about 6–8000 sections per brain) were obtained (coronal sections, thickness 20 µm). During sectioning, block-face images after each 15th section were registered using a CCD camera. Sections were mounted on glass slides and the cell bodies were stained using a modified silver staining method (Merker 1983). Every 60th coronal section of each brain's entire histological series was digitized, and subjected to cytoarchitectonic analysis resulting in a distance of 1.2 mm between analyzed sections. The MR sequences of the fixed brain, the block-face images, and the digitized histological sections were used to create 3D reconstructed histological volumes of each brain, corrected for distortions by registration to the MR volume of the respective brain (e.g., Amunts et al. 2000).

Nomenclature

The nomenclature of the cytoarchitectonic areas is distinct from functionally based nomenclatures to indicate the methodological basis (cytoarchitecture), the species (h indicates human brain) and the topography (Oc-occipital lobe, number “4” the fourth area when moving rostrally from the primary visual area (BA 17/V1/hOc1), letter “l” lateral, while “a” and “p” indicate anterior and posterior locations).

Observer-independent and statistically testable detection of cytoarchitectonic borders

The borders between cytoarchitectonic areas were defined using an algorithm-based approach introduced by Schleicher et al. (1999, 2000, 2005). The cytoarchitecture was analyzed in cortical regions of interest (ROIs) along the surface of the LOC. The ROIs were partially surrounded at the rostral extent by area hOc5 (Malikovic et al. 2007) located immediately behind the anterior occipital sulcus, at the dorsal side by areas hOc3d and hOc4d (Kujovic et al. 2013) related to the superior occipital and transverse occipital sulcus, and at the ventral part by areas hOc3v and hOc4v (Rottschy et al. 2007) closely related to the inferior occipital sulcus (Figs. 1, 2a, b, 4a).

The ROIs were defined in histological sections and scanned using a microscope (Zeiss, Germany) with a motorized scanning stage and a CCD camera (Sony, Tokyo, Japan) resulting in an in-plane resolution of 1 µm per pixel. The digitized sections were transformed to gray level index (GLI) images using a KS400® image analyzing system (Zeiss, Oberkochen, Germany). The gray level index quantifies the volume fraction of cell bodies for each measuring field (Schleicher and Zilles 1990; Wree et al. 1982) (Figs. 2, 3). The size of each measuring field was 17 × 17 µm. The GLI images were further used to generate GLI profiles.

The GLI profiles were extracted as measures of cytoarchitecture along curvilinear trajectories oriented perpendicular to the cortical layers and surface, and extended from the outer contour (border of layer I/II) to the inner contour (layer VI/subcortical white matter border) (Figs. 2b, c, d, 3b, c, d). Curvilinear trajectories follow the distortions of the cortical columns, caused by cortical folding, offering better results than straight trajectories (Jones et al. 2000; Schleicher et al. 2005; Schmitt and Böhme 2002). The GLI profiles were standardized to the

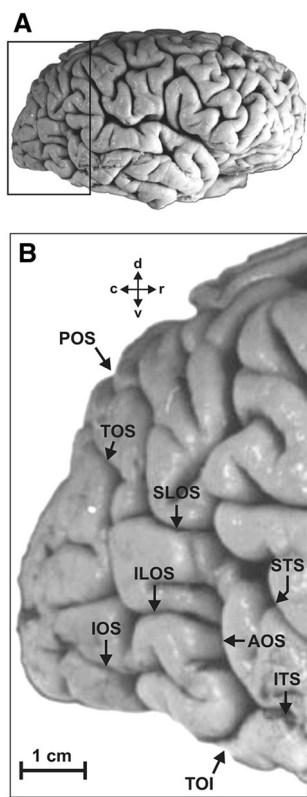


Fig. 1 **a** Lateral surface of brain number 3, right hemisphere. **b** Main sulci of the lateral occipital cortex and related temporal sulci. *AOS* anterior occipital sulcus, *ILOS* inferior lateral occipital sulcus, *IOS* inferior occipital sulcus, *ITS* inferior temporal sulcus, *POS* parieto-occipital sulcus, *SLOS* superior lateral occipital sulcus, *STS* superior temporal sulcus, *TOI* temporo-occipital incisure, *TOS* transverse occipital sulcus. Cross arrow: *c* caudal, *d* dorsal, *r* rostral, *v* ventral

cortical thickness of 100 % to normalize variations in cortical thickness. The shape of these profiles was quantified using a 10-dimensional feature vector which included the following parameters: mean GLI value, the cortical depth of the profile's gravity center, the standard deviation, the skewness, the kurtosis of the profile, as well as the analogous parameters for the first derivative of the profile (Schleicher et al. 1999). The positions of the GLI profiles along the cortical surface of each ROI were numbered from 1 to n (n indicates the total number of profiles per ROI).

The borders between cytoarchitectonic areas were identified by significant changes of the feature vectors between blocks of neighboring GLI profiles (distance between profiles 90 μm). A multivariate distance measure (Mahalanobis distance, D^2), that defines the difference between the neighboring GLI profiles, was used to reveal these differences (Mahalanobis et al. 1949; Schleicher et al. 2000, 2005), and reflects transitions in laminar patterns between two cytoarchitectonic areas. The statistical significance of the transitions was tested with Hotellings T^2 tests and Bonferroni correction (Bartels 1979).

During the identification of areal borders, neighboring blocks of GLI profiles were moved as sliding windows along the cortex in steps of one profile position (~90 μm). A D^2 was calculated for each position. This sliding window procedure was repeated for block sizes ranging from 8 to 24 profiles. The Mahalanobis distance showed maxima at locations where the shape of the GLI profiles changed. The maxima were interpreted as revealing cortical borders when they were detected and reached significance throughout most block sizes, and could be reproduced at a comparable position along the cortical ribbon in several neighboring sections. In house software based on MATLAB® (MathWorks, USA) was used to define the areal borders and test their statistical significance (Schleicher et al. 1999). Borders were identified using 4–15 ROIs per hemisphere. The results of observer-independent detection of cytoarchitectonic borders were microscopically confirmed.

Despite the significant changes in the shape of GLI profiles between cortical areas, the profiles *within* a cortical area show some variability, which leads to a “noisy” course of the Mahalanobis distance curve visible by interposed local maxima (Figs. 2, 3). This “noisy” course was also found to more or less extent in previous observations of the primary and secondary visual cortex, inferior parietal lobule, intraparietal sulcus, and extrastriate areas (Amunts et al. 2000; Caspers et al. 2006; Choi et al. 2006; Kujovic et al. 2013; Rottschy et al. 2007). The mean distance between the local maxima of the Mahalanobis curve is about 2.5 mm in the present observation. Since these relatively regular undulations of the Mahalanobis curve are in sharp contrast to the significant maxima by the fact that they cannot be observed at comparable positions over a longer distance in adjacent sections, they probably indicate patch-like variations of cytoarchitecture within a cortical area and are not indicative of an interareal border. The patch-like organization of the microstructure within cortical areas caused by interdigitating input from different sources has been repeatedly described in the past in various cortical regions (e.g., Goldman and Nauta 1977; Goldman-Rakic 1984, 1995; Goldman-Rakic and Schwartz 1982).

Principal component and hierarchical cluster analyses

To further evaluate the parcellation based on the observer-independent approach, a principal component analysis and a hierarchical cluster analysis (Euclidean distances and Ward linkage) were performed with feature vectors extracted from the GLI profiles of 11 visual areas separated by hemispheres. The following areas were included: hOc4la, hOc4lp (present observation), V1 and V2 (Amunts et al. 2000), hOc3v and hOc4v (Rottschy et al. 2007),

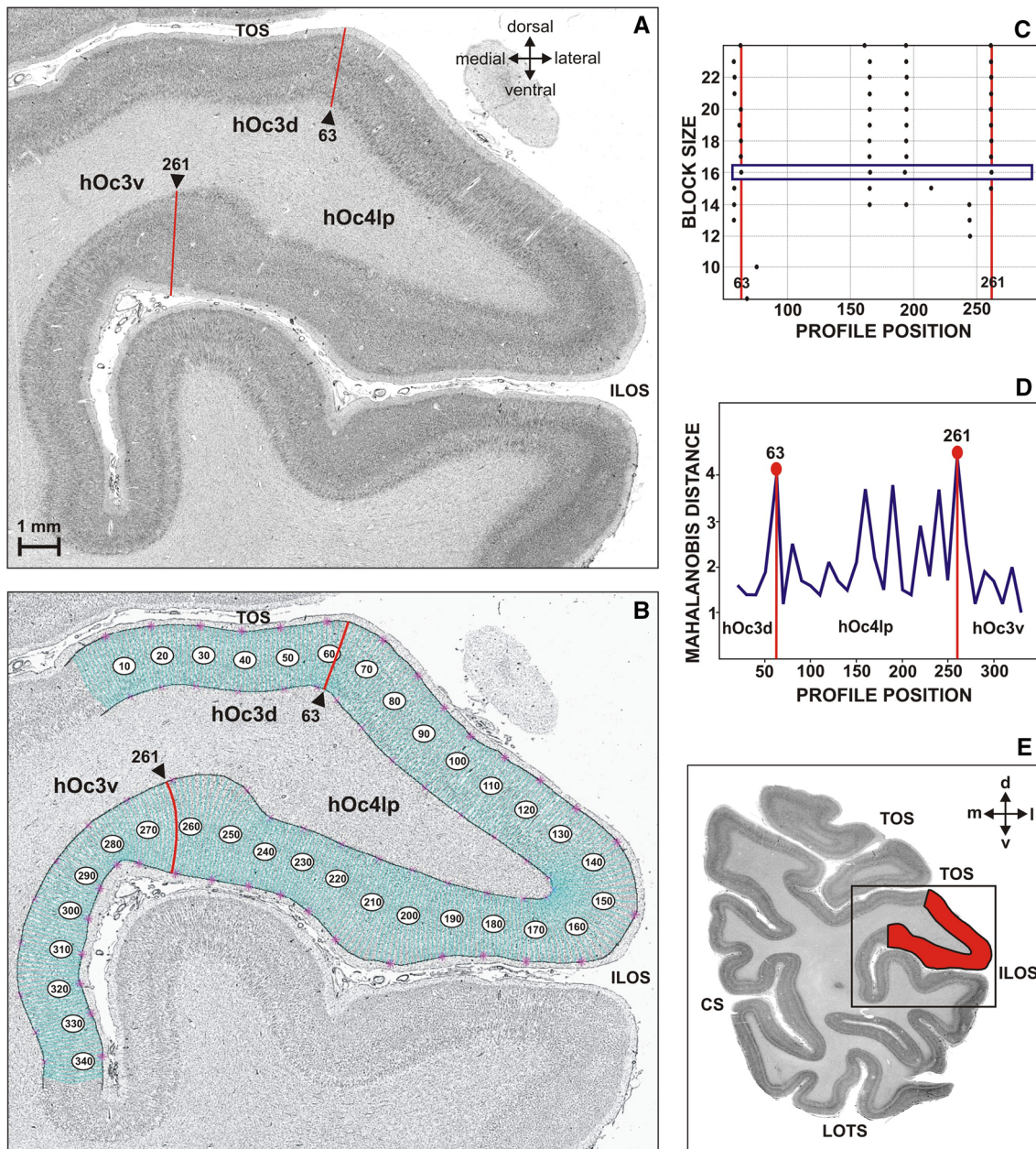


Fig. 2 Observer-independent definition of cortical borders of area *hOc4lp* in an exemplary coronal, histological section stained for cell bodies. **a** Cytoarchitecture of area *hOc4lp*. Solid red lines and arrowheads mark the borders between *hOc4lp* and neighboring areas *hOc3d* and *hOc3v*. **b** Curvilinear traverses were computed perpendicular to the cortical layers of the lateral occipital cortex. The GLI profiles (numbered from 1 to 345) were extracted along these traverses in order to detect cortical borders. **c** Mahalanobis distances

between adjacent blocks of GLI profiles were calculated by using a sliding window of different sizes: those for a block size of 16 are highlighted in blue. **d** Significant maxima of Mahalanobis distances (at profile positions 63 and 261) indicate cortical borders. Borders of *hOc4lp* were found at positions 63 (*hOc4lp/hOc3d* border) and 261 (*hOc4lp/hOc3v* border). **e** Location of area *hOc4lp* (red) in the histological section. Cross arrow: *d* dorsal, *l* lateral, *m* medial, *v* ventral

hOc3d and *hOc4d* (Kujovic et al. 2013), *hOc5* (Malikovic et al. 2007), and *FG1* and *FG2* (Caspers et al. 2013). The meaningful number of clusters was defined using Silhouette analysis. Statistics and visualization were carried out with in house R-scripts (R Foundation for Statistical Computing, <http://www.r-project.org>).

Definition of areal volumes

Identified cytoarchitectonic areas *hOc4la* and *hOc4lp* were labeled in high-resolution images of histological sections (spatial resolution of the digitized images, 7000×6000 pixels). Areal Volumes (V , in mm^3) were calculated from

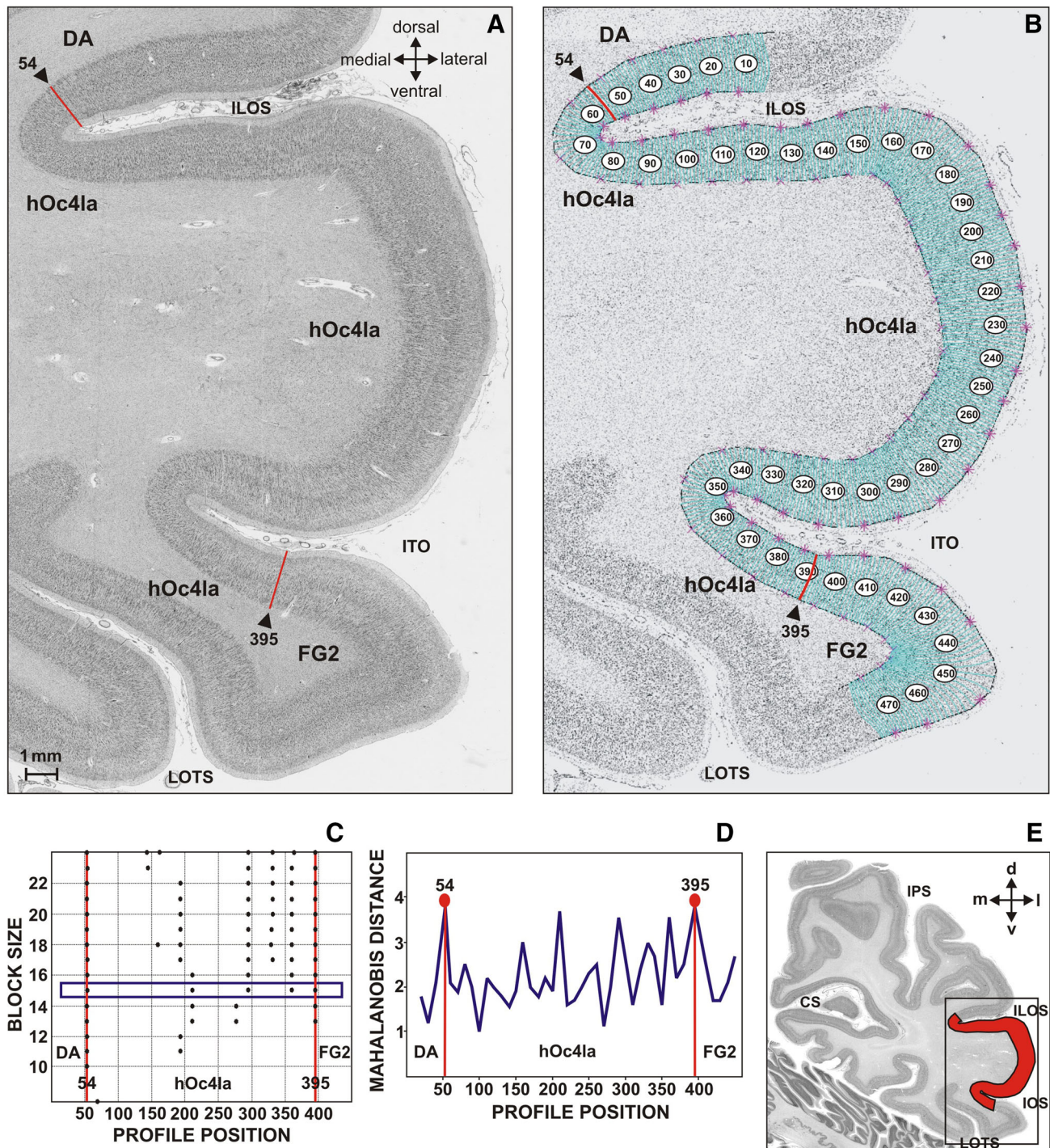


Fig. 3 Observer-independent definition of cortical borders of area hOc4la in an exemplary coronal, histological section stained for cell bodies. **a** Cytoarchitecture of area hOc4la. Solid red lines and arrowheads mark the borders between area hOc4la and the dorsally adjacent not further delineated area DA and the ventrally located area FG2. **b** The GLI profiles (numbered from 1 to 476) were extracted along the curvilinear traverses for the detection of cortical borders.

c Mahalanobis distances between adjacent blocks of GLI profiles were calculated (those for a block size of 15 are highlighted in blue). **d** Significant maxima of Mahalanobis distances that indicate borders of area hOc4la have been found at positions 54 (hOc4la/dorsal area border) and 395 (hOc4la/FG2 border). **e** Location of area hOc4la (red) in the histological section. Cross arrow: *d* dorsal, *l* lateral, *m* medial, *v* ventral

area measurements (A_i) in the 3D reconstructed histological sections using the following formula:

$$V = (s \times T) \times x \times y \times \Sigma A_i \times F$$

where s is the distance between two measured sections (number of sections), T is the thickness of a histological sections (0.02 mm), x is the width of a pixel (0.0212 mm) and y is the height of a pixel in the image (0.0212 mm), ΣA_i is the sum of pixels across all evaluated sections, and F is the individual shrinkage factor of the brain.

Depending on the extent of each area (hOc4la and hOc4lp), eight to 14 sections were analyzed per hemisphere and brain. The volumes of areas hOc4la and hOc4lp were compared between hemispheres (inter-hemispheric differences) and between male and female brains (gender differences) using an analysis of variance (ANOVA) with a repeated-measure design.

Continuous probabilistic cytoarchitectonic mapping in stereotaxic space

The histological volumes of the post-mortem brains were 3D reconstructed (Amunts et al. 2004), and the cytoarchitectonic areas were interactively traced in the corresponding sections of the reconstructed volume. The reconstructed volumes were spatially normalized to the T1-weighted single subject reference space of the Montreal Neurological Institute, the MNI space (Collins et al. 1994; Evans et al. 1993; Holmes et al. 1998) using a combination of affine and nonlinear, elastic registration transformations (Amunts et al. 2004; Henn et al. 1997; Hömke 2006). Since the origin of the MNI space does not coincide with the location of the anterior commissure (Talairach and Tournoux 1988), we transformed our data to the anatomical MNI space (Amunts et al. 2005). The anatomical MNI space differs from the original MNI space by a linear shift of the origin in rostro-caudal (shifted 4 mm more caudally) and ventro-dorsal (shifted 5 mm more dorsally) directions. The origin and orientation of the anatomical MNI space accord with the convention of Talairach and Tournoux (1988).

Following spatial normalization, individual volumes of areas hOc4la and hOc4lp were registered to the 3D reference space and anatomical continuous probabilistic maps were generated for both areas (Amunts and Zilles 2001; Eickhoff et al. 2007; Zilles et al. 2002). These maps reflect the relative frequency of areas hOc4la and hOc4lp in each voxel of the 3D reference space (anatomical MNI space). The degrees of overlap were color coded for both areas. Centers of gravity of these maps were positioned in the anatomical MNI space for each hemisphere and brain. Additionally, maximum probability maps (MPM) of areas hOc4la and hOc4lp were generated for the meta-analysis of connectivity and functional properties (see below). These

maps identify the most likely anatomical area in each voxel of the 3D reference space and provide non-overlapping maps (Eickhoff et al. 2005).

The anatomical probability maps and maximum probability maps of areas hOc4la and hOc4lp are available http://www.fz-juelich.de/inm/inm-1/EN/Home/home_node.html and through the JuBrain web viewer (<https://www.jubrain.fz-juelich.de/apps/cytoviewer/cytoviewer-main.php>). They can easily be applied using the anatomy toolbox (Eickhoff et al. 2005) developed for the application of cytoarchitectonic anatomical probability maps as an option integrated in the SPM software (www.fil.ion.ucl.ac.uk/spm). The toolbox can be downloaded <https://www.jubrain.fz-juelich.de/apps/cytoviewer/cytoviewer-main.php>.

Connectivity and functional properties of areas hOc4la and hOc4lp

Functional connectivity of hOc4la and hOc4lp was analyzed by meta-analytic connectivity modeling (MACM). The maps of the cytoarchitectonically defined areas served as seeds. This approach to functional connectivity assesses which brain regions are co-activated above chance with a particular seed region in functional neuroimaging experiments. To this end, we employed the BrainMap database (Laird et al. 2009, 2011) (www.brainmap.org), which contained at the time of analysis approximately 10,000 neuroimaging experiments. We only included studies that reported group analyses of functional mapping experiments of healthy subjects, yielding approximately 7500 experiments for analysis. To delineate task-based functional connectivity, i.e., co-activations of hOc4la and hOc4lp, we first identified all experiments in the BrainMap database that featured at least one focus of activation in the respective area. Subsequently, the convergence of foci reported in these experiments was quantified using the revised Activation Likelihood Estimation (ALE) algorithm (Eickhoff et al. 2009). The key idea behind ALE is to model the reported foci as 3D Gaussian probability distributions capturing the spatial uncertainty associated with them. These probabilities are then combined to yield voxel-wise ALE scores describing the convergence across experiments. To distinguish ‘true’ convergence between experiments from random convergence (i.e., noise), ALE scores were compared to a null-distribution reflecting random spatial association (Eickhoff et al. 2012). The p value of each experimental ALE value is then given by the proportion of equal or higher values obtained under the null distribution and the MACM results were thresholded at a cluster-level corrected threshold of $p < 0.05$ (cluster-forming threshold at voxel-level $p < 0.001$).

Difference maps comparing task-based functional connectivity maps of areas hOc4la and hOc4lp were

established by first calculating the voxel-wise differences of the z-scores obtained from the inspected MACM maps. The experiments contributing to either analysis were then pooled and randomly divided into two groups of the same size as the sets of contrasted experiments (Eickhoff et al. 2011). Voxel-wise ALE scores for these two randomly assembled groups were subtracted from each other and recorded. Repeating this process 10,000 times yielded an empirical null distribution of ALE score differences between the two conditions. Based on this permutation-procedure, the map of true differences was then thresholded at a posterior probability of $p > 0.95$ for a true difference between the two samples. The resulting maps were then masked with the respective main effect of the minuend connectivity map to avoid obtaining significant connectivity in voxels of the difference map that do not show significant co-activation on the underlying connectivity map (Rottschy et al. 2012).

To identify functional properties and connectivity of areas hOc4la and hOc4lp, we performed, separately for each area, meta-analytic connectivity modeling (MACM) and quantitative functional decoding across a large database of functional neuroimaging studies. The seed regions of the lateral occipital cortex were defined by the anatomical locations of cytoarchitectonic areas hOc4la and hOc4lp using their maximum probability map representations in MNI space.

The functional characterization of areas hOc4la and hOc4lp was based on the BrainMap meta-data that describes the classes of mental processes isolated by the archived experiments' statistical contrasts. In this context, behavioral domains denote the mental processes isolated by the respective contrast, whereas paradigm classes categorize the specific task employed (see <http://brainmap.org/scribe/> for the complete BrainMap taxonomy). Functional decoding was then based on analyzing the behavioral domains and paradigm classes' meta-data associated with the experiments activating areas hOc4la and hOc4lp, respectively. In particular, we assessed the frequency of domain "hits" relative to its likelihood across the entire database (Rottschy et al. 2012). Functional roles for each area were then identified by significant over-representation of behavioral domains and paradigm classes in the BrainMap experiments associated with a respective area relative to the BrainMap database. The base rate is the a priori probability of any focus to lie in the respective area. The conditional probability of seed-term associations was then computed and compared to the base rate using a binomial test ($p < 0.05$), corrected for the false discovery rate within multiple comparisons. This allowed characterizing the functional profile of a seed by identifying taxonomic terms, for which the probability of finding activation in the respective seed was significantly higher as compared to the

term's baseline (Cieslik et al. 2013; Kellermann et al. 2013; Reetz et al. 2012).

Results

Cytoarchitecture and borders of lateral occipital areas hOc4la and hOc4lp

We delineated two new cytoarchitectonic areas, hOc4la and hOc4lp, in the region of the lateral occipital cortex (Fig. 4). The cytoarchitecture of each area is distinct and differs from those of neighboring areas. hOc4la (anterior lateral occipital area) differs from the neighboring occipital areas by higher cell-packing density in its granular layers (II and IV), less prominent layer III with larger cells in its sublayer IIIb and higher cell-packing density in layers V and VI. Layer II is broad with smaller cells, and its border with sublayer IIIa is more prominent. The thickness of layer III is slightly reduced, and its segmentation into sublayers is less obvious, because the pyramidal cells in sublayer IIIb are similar in size to those in sublayer IIIc. Layer IV is located slightly higher compared to the neighboring occipital areas, and its small cells form irregular columns that penetrate into layers III and V. Layer V is composed of two sublayers (Va and Vb), and its cell-packing density is lower than that of layer VI, but the cells of layer V are slightly larger. The border between layers V and VI is less pronounced, because the cell-packing density of sublayer Vb increases (compared to sublayer Va) approaching those observed in layer VI (Figs. 5a, 6a, b, 7a, b).

hOc4lp (posterior lateral occipital area) is characterized by a prominent layer III, with a clear radial arrangement and larger pyramidal cells in sublayer IIIc and lower cell-packing density in layer V. Granular layers II and IV have a lower cell-packing density than anterior area hOc4la, and the border between layers II and III is less clear. Layer III is broad, with densely packed cells arranged in radial columns. It is composed of three sublayers (IIIa, IIIb and IIIc), and pyramidal cells in these sublayers increase gradually in their size from sublayer IIIa to IIIc. Pyramidal cells in sublayers IIIb and IIIc are smaller than those in area hOc4la. Layer IV is located slightly lower than in hOc4la, and layers V and VI are narrower and less densely packed in area hOc4lp than in area hOc4la. Neurons in sublayer Va are smaller than those of area hOc4la, and sublayer Vb of area hOc4lp is less densely packed, which makes the border between layers V and VI more pronounced (Figs. 5b, 8a–c, 9a, b).

hOc4la shares common borders with occipital extrastriate areas hOc4lp (Fig. 6a), hOc5 and hOc4v (Fig. 6b). hOc4la borders hOc5 (Malikovic et al. 2007) along the

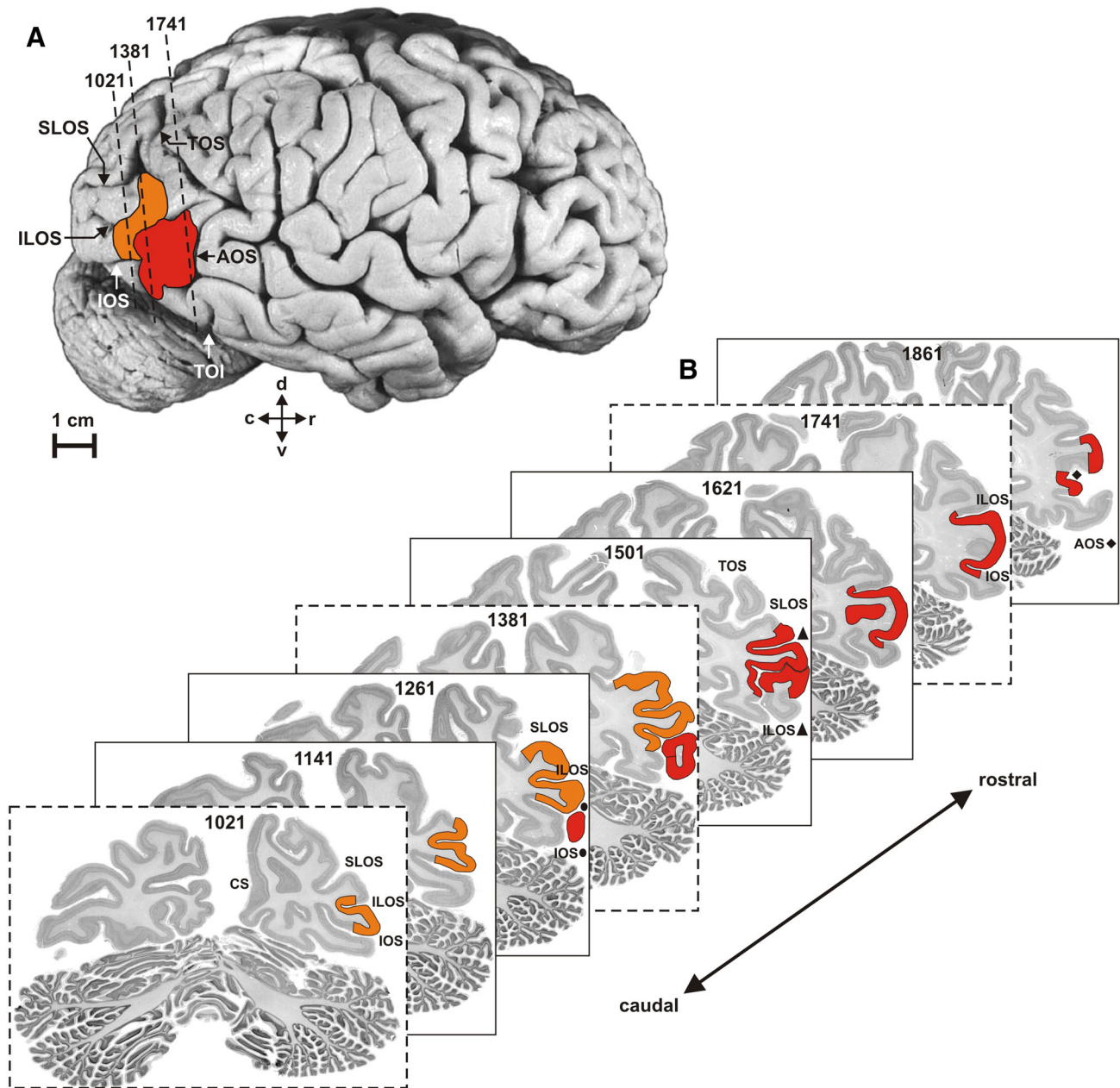


Fig. 4 Location and extent of areas hOc4la (red) and hOc4lp (orange) on the surface of brain number 10 (a) and in a selection of histological serial sections (b). The dashed lines in panel a show the approximate level of Section 1021, 1381 and 1741 in panel B. AOS anterior occipital sulcus, CS calcarine sulcus, ILOS inferior

lateral occipital sulcus, IOS inferior occipital sulcus, SLOS superior lateral occipital sulcus, TOI temporo-occipital incisure, TOS transverse occipital sulcus. Cross arrow: c caudal, d dorsal, r rostral, v ventral

anterior part of the lateral occipital cortex. Compared with hOc5, area hOc4la shows a larger mean size of pyramidal cells in sublayers IIIb and IIIc, a higher cell-packing density in layers V and VI and larger pyramidal cells in layer V. hOc4la borders in part the ventrally located area hOc4v (Rottschy et al. 2007) along the inferolateral margin of the occipital lobe. Compared with hOc4v, area hOc4la has larger pyramidal cells in sublayer IIIb, more densely

packed cells in layers V and VI and larger cells in layer VI. The thickness of layer III, as well as the size of pyramidal cells in sublayers IIIa and Va, are similar in both occipital extrastriate areas (Fig. 6b).

Not further delineated is an area in the region of the parieto-temporo-occipital junction and dorsal to the anterior part of hOc4la. This area, which we labeled DA, has a higher cell-packing density in layers II, III and IV than

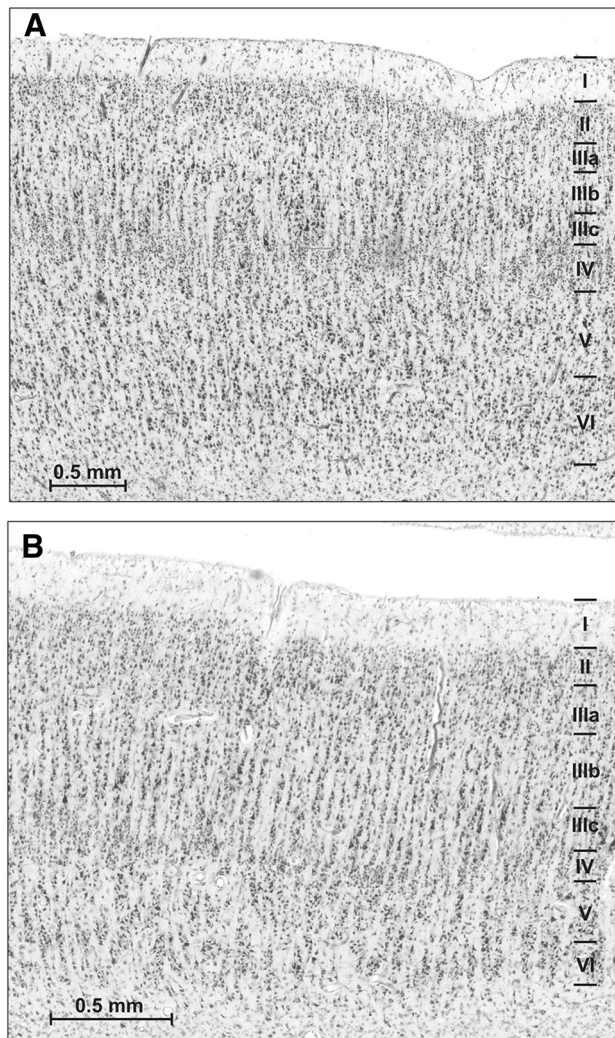


Fig. 5 Cytoarchitecture of areas hOc4la (a) and hOc4lp (b). Roman numerals indicate cortical layers

hOc4la. In DA, layer III is less prominent with a cell-packing density more similar across sublayers and with smaller pyramidal cells than in hOc4la. Layer V is more densely packed compared to hOc4la, and its cells are smaller than those in layer VI (Fig. 7a).

In the region of the temporo-occipital junction and ventral to the anterior part of hOc4la, area FG2 is visible (Caspers et al. 2013), which extends further into the inferior temporal cortex. Compared to hOc4la, area FG2 has a higher cell-packing density in layers II, IIIa and IV, smaller pyramidal cells in sublayer IIIc and more densely packed layers V and VI. Sublayer IIIb of FG2 is lower in cell-packing density and layer VI can be separated in two sublayers: VIa and VIb (Fig. 7b).

hOc4lp shares common borders with occipital extrastriate areas hOc3d, hOc4d, hOc3v, hOc4v and hOc4la (Figs. 8a–c, 9a, b). hOc4lp borders areas hOc3d and hOc4d

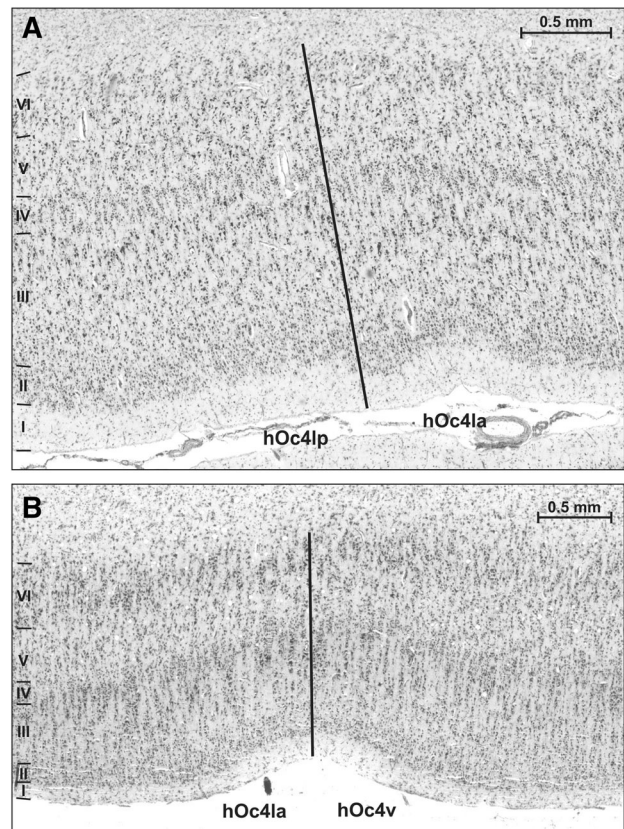


Fig. 6 a Border between areas hOc4la and hOc4lp, b Border between areas hOc4la and hOc4v (Rottschy et al. 2007). Roman numerals indicate cortical layers

along the dorsal part of LOC. The cytoarchitecture of hOc4lp differs from that of area hOc3d by a less pronounced radial cellular arrangement, less uniform cell-packing density through the whole cortical thickness, larger pyramidal cells in sublayers IIIb, IIIc and Va, and more densely packed layers V and VI (Fig. 8a). The border between hOc4lp and hOc4d is characterized by a lower cell-packing density in layers II and IIIa and smaller pyramidal cells in sublayers IIIb and IIIc in area hOc4lp. Layer IV of hOc4lp is located slightly higher, and the thickness of layer III is slightly reduced compared to hOc4d. The thickness of layers V and VI is greater in hOc4lp and pyramidal cells in layer V are smaller than those in hOc4d. Layer VI is more densely packed in hOc4d than in hOc4lp, and the border between layer VI and subcortical white matter is more pronounced (Fig. 8b).

hOc4lp borders areas hOc3v and hOc4v along the ventral part of LOC (Fig. 9a, b). Compared to hOc3v, area hOc4lp has lower cell-packing density in layers II, IIIa and IV, a more densely packed layer V and larger pyramidal cells in sublayers IIIa and IIIb. The thickness of layers V and VI is greater in hOc4lp, while the thickness of layer III is reduced compared to area hOc3v (Fig. 9a). The border

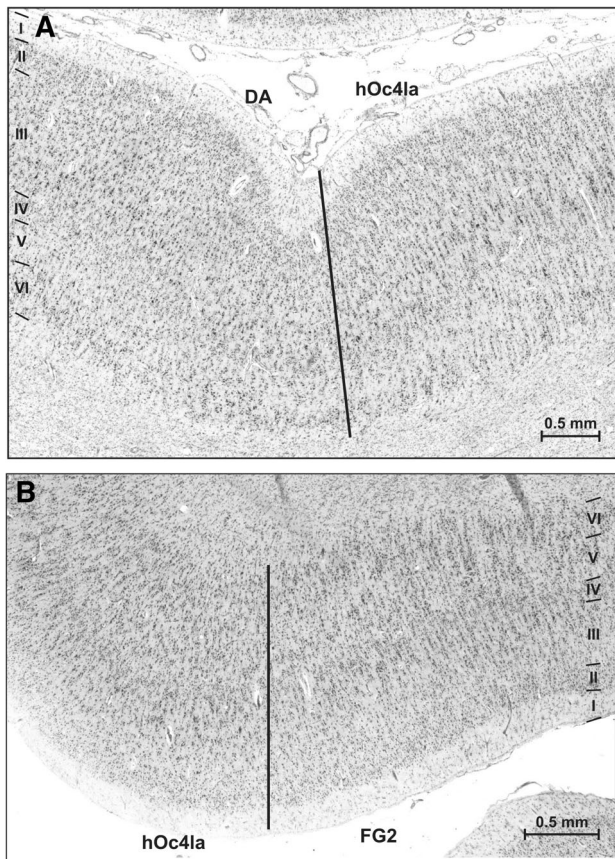


Fig. 7 **a** Border between area hOc4la and the not further delineated cortical area DA located dorsal to area hOc4la. **b** Border between area hOc4la and area FG2 (Caspers et al. 2013). Roman numerals indicate cortical layers

between hOc4lp and hOc4v is characterized by lower cell-packing density in layers II, III, IV and Va, and smaller pyramidal cells in sublayers IIIb, IIIc and Va in area hOc4lp. The thickness of layer III in both areas is approximately equal (Fig. 9b).

A here not further delineated area DA (Fig. 8c) with higher cell-packing density in layers II, IV and V and smaller pyramidal neurons in sublayers IIIb and IIIc is also found dorsal to hOc4lp. Layer III of that area is more uniform in cell-packing density and size of cells across its sublayers. The average size of its pyramidal cells in deeper layer III and Va is approximately equal.

Location with respect to the gross anatomical landmarks

hOc4la is located in rostral and ventral portions of LOC behind the anterior occipital sulcus. hOc4la occupies the anterior thirds of the middle and inferior lateral occipital gyrus divided by the inferior lateral occipital sulcus. The most ventral part of hOc4la extends behind and above to

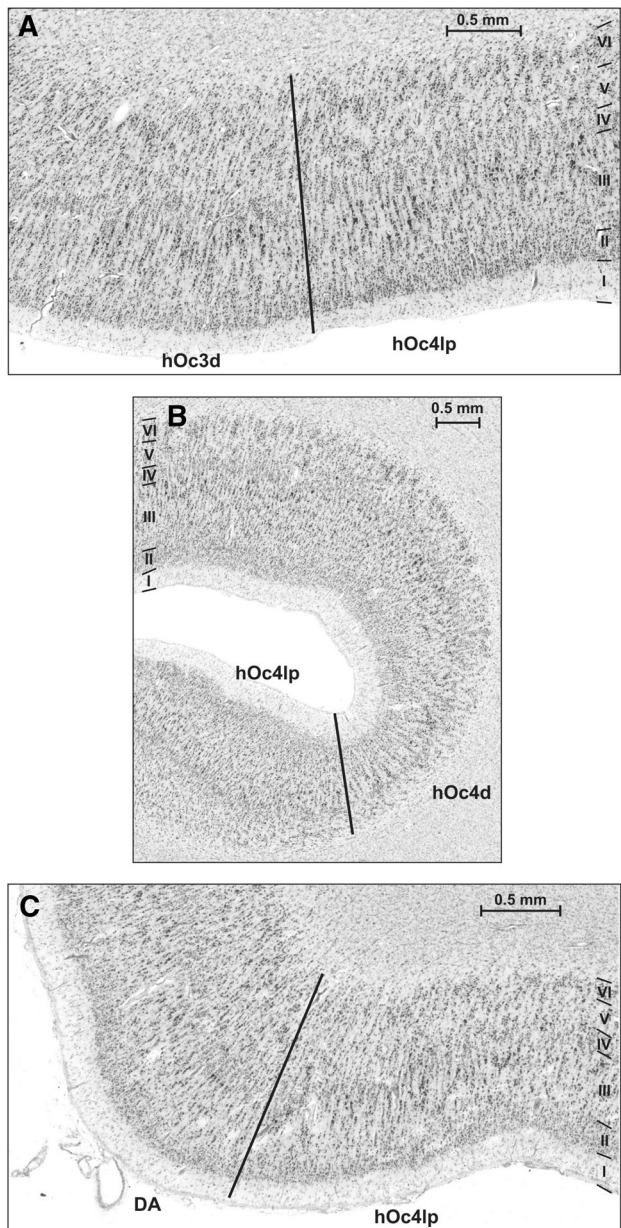


Fig. 8 **a** Border between area hOc4lp and area hOc3d (Kujovic et al. 2013). **b** Border between area hOc4lp and area hOc4d (Kujovic et al. 2013). **c** Border between area hOc4lp and the not further delineated dorsal area DA. Roman numerals indicate cortical layers

the temporo-occipital incisure (preoccipital incisure) and the inferolateral margin of the occipital lobe (in 18 out of 20 hemispheres). In the remaining 2 hemispheres, the most ventral part of area hOc4la reaches the temporo-occipital incisure, extending just above to the inferolateral margin of the occipital lobe.

hOc4lp occupies the caudal and dorsal portions of the lateral occipital cortex where it extends along the superior and middle lateral occipital gyri, divided by the inconstant superior occipital lateral sulcus (Malikovic et al. 2012). In

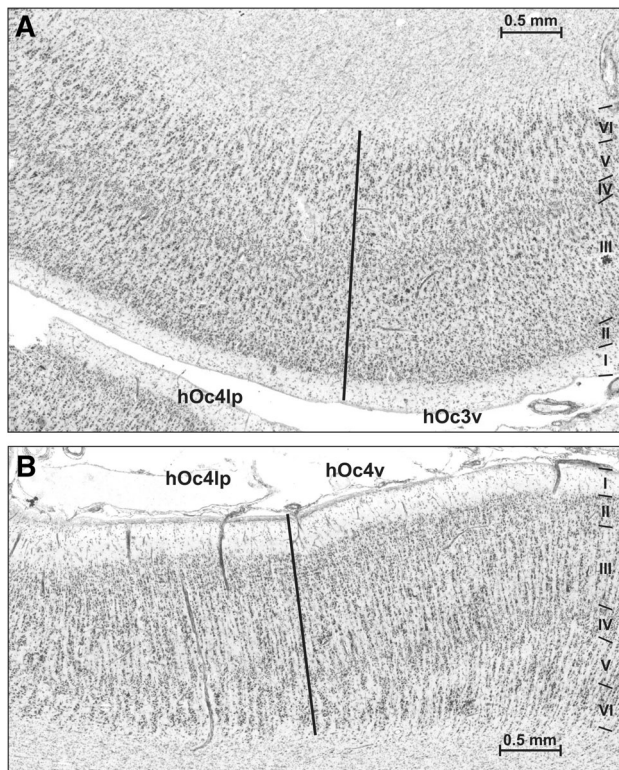


Fig. 9 **a** Border between area hOc4lp and area hOc3v (Rottschy et al. 2007). **b** Border between area hOc4lp and area hOc4v (Rottschy et al. 2007). Roman numerals indicate cortical layers

most of cases (15 out of 20 hemispheres), the dorsal part of area hOc4lp is located behind the transverse occipital sulcus. (Figs. 1b, 4a, b).

Location with respect to adjacent cytoarchitectonic areas

hOc4la is located immediately behind the area hOc5 (Malikovic et al. 2007). hOc4la hooks around the caudal half of the area hOc5 (Fig. 10). hOc4la shares common borders with two extrastriate areas at its caudal border: hOc4lp and hOc4v (Rottschy et al. 2007). Finally, hOc4la shares a common border with the area FG2 (Caspers et al. 2013) in the region of the temporo-occipital incisure along the inferolateral margin of the occipital lobe. FG2 is located ventral and rostral of hOc4la in the region of the posterior fusiform gyrus extending along its lateral portion.

hOc4lp is located immediately behind the area hOc4la. Areas hOc4d and hOc3d (Kujovic et al. 2013) are located dorsal and caudal to the area hOc4lp, respectively. Ventral to the area hOc4lp, there are three extrastriate areas, V2 (Amunts et al. 2000), hOc3v and hOc4v (Rottschy et al. 2007) (Fig. 10).

Figure 10 depicts the extent in ten brains of the areas hOc4la and hOc4lp and of all other visual areas which have

been cytoarchitectonically identified using the same method. Although the topographical relation between the areas is consistent in all brains, a considerable inter-subject variability in extent and position of the areas can be seen. This will be further analyzed by calculating continuous probability maps (see below).

Cluster analyses of cytoarchitectonic areas

The cytoarchitecture quantified by GLI profiles is studied across hemispheres using hierarchical cluster and principal component analyses. This allows the validation of the delineation of cytoarchitectonic areas and to further expand on the question of cytoarchitectonic clusters between and within regions. The analyses separately for the right and left hemispheres and areas V1, V2, hOc3d, hOc3v, hOc4d, hOc4v, hOc4la, hOc4lp, hOc5, FG1 and FG2 demonstrates:

- These visual areas form four clusters with the primary (V1) and secondary (V2) visual cortex in one cluster, areas hOc3d, hOc4d and hOc5 in another cluster, areas hOc3v and hOc4v in a third cluster, and areas hOc4la, hOc4lp, FG1 and FG2 in a fourth cluster (Fig. 11a). It shows that the very early visual areas V1 and V2 clearly differ from the other three clusters. Furthermore, the dorsal stream areas in cluster 2 greatly differ from the other clusters, whereas the areas in clusters 3 and 4 are relatively close to each other in the principal component analysis.
- The hierarchical cluster analysis (Fig. 11b) supports the result of the principal component analysis. In most cases, the same cytoarchitectonic area on the left and right hemisphere is closer aligned than different areas in the same hemisphere. There are some exceptions, e.g., hOc3v and hOc4v in each hemisphere seem to be more similar to each of these areas across hemispheres. Left hOc4la seems to be more similar to FG2 than to right hOc4la. Finally, right V2 seems to be more similar to left and right V1 than to left V2. These seemingly exceptions must be interpreted, however, with some caution, because the Silhouette analysis predicts an optimal number of four clusters, which means, that the examined areas cannot be separated at the level of hemispheres. This is probably so because the GLI profiles do not provide a signal to noise ratio strong enough to reach significant levels of similarity or dissimilarity. Therefore, both analyses demonstrate that the observer-independent approach enables a quantitatively based parcellation which clearly separates different cytoarchitectonic areas and enables a hierarchical positioning of the areas.
- A comparison of profiles extracted from several sectors within both hOc4la and hOc4lp does not support a significant dissimilarity in cytoarchitecture of such sectors within each of these areas.

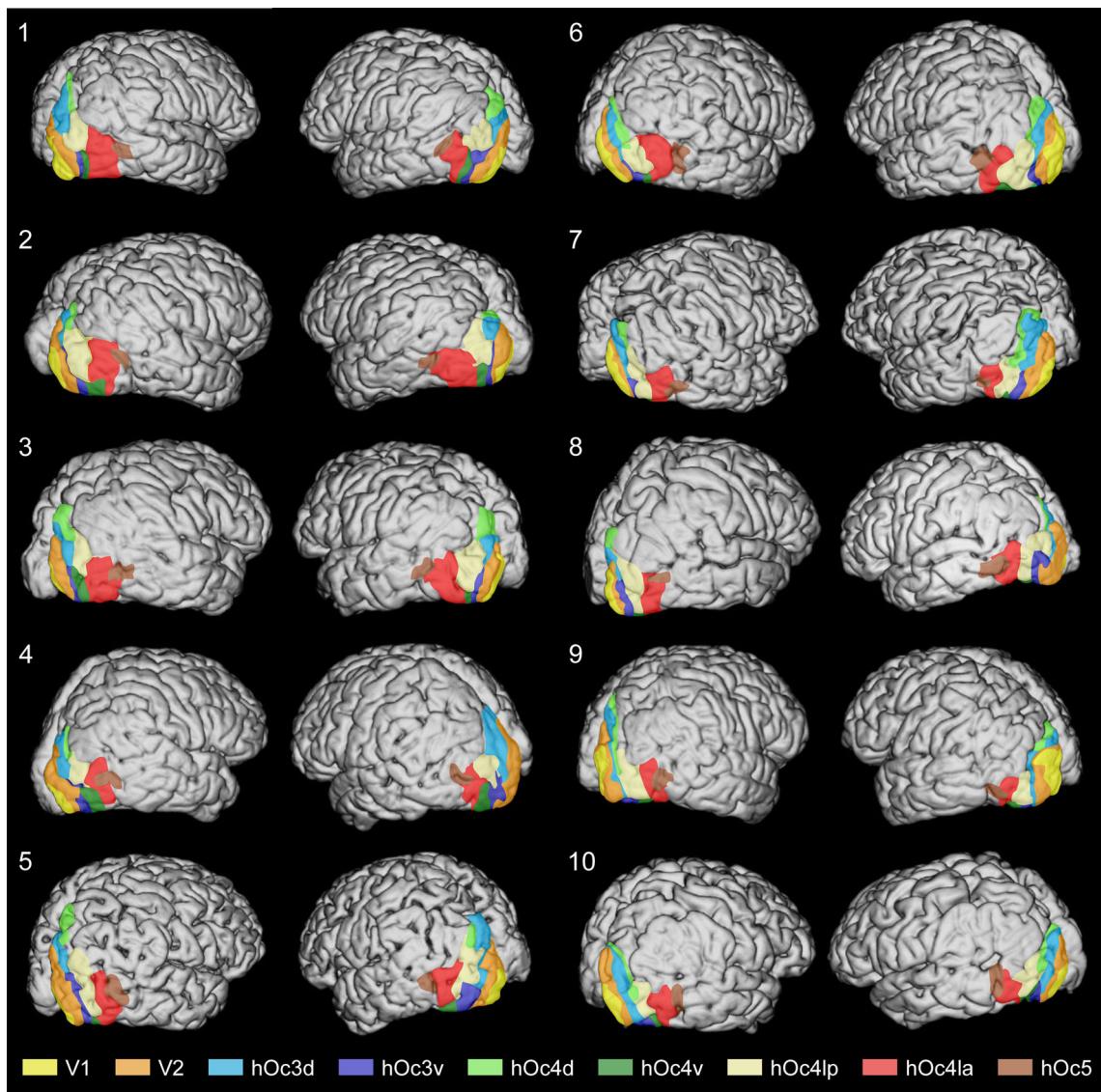


Fig. 10 Position and extent of cytoarchitectonically defined visual areas in the *left* and *right hemispheres* of ten human brains. The lateral view of all hemispheres is given in a slightly oblique perspective from a posterior and dorsal position

Volumes of areas hOc4la and hOc4lp

The mean volume of area hOc4la, measured in all 20 hemispheres is 2.61 cm^3 (SD 0.89). The mean right volume (measured in 10 right hemispheres) of hOc4la is slightly, but not significantly ($p > 0.05$) larger (2.81 cm^3 , SD 0.97) than that of the left side (2.42 cm^3 , SD 0.79). Eight out of ten brains show a larger mean volume of area hOc4la in the right than in the left hemisphere. The individual volumes of area hOc4la vary between 1.45 and 4.28 cm^3 in the right hemisphere (factor of 2.9), and between 1.37 and 4.01 cm^3 in the left (factor of 2.9).

The mean volume of hOc4lp (measured in all 20 hemispheres) is 2.39 cm^3 (SD = 0.59), and is slightly smaller

(0.22 cm^3) compared to that of area hOc4la. The mean left volume (measured in 10 left hemispheres) of hOc4lp is significantly ($p < 0.05$) larger (2.64 cm^3 , SD 0.81) than that of the right side (2.13 cm^3 , SD = 0.37). Nine out of ten brains have larger mean volumes of area hOc4lp in the left than in the right hemisphere. The individual volumes of area hOc4lp vary between 1.74 and 4.09 cm^3 in the left (factor of 2.3), and between 1.72 and 2.59 cm^3 in the right hemisphere (factor of 1.5). The mean volume of both lateral occipital areas, hOc4la plus hOc4lp, is larger in male than in female brains, but this difference is not significant ($p > 0.05$). The absolute volumes and the relative volumes (normalized by brain weight) of hOc4la and hOc4lp did not show any consistent change with age in our sample.

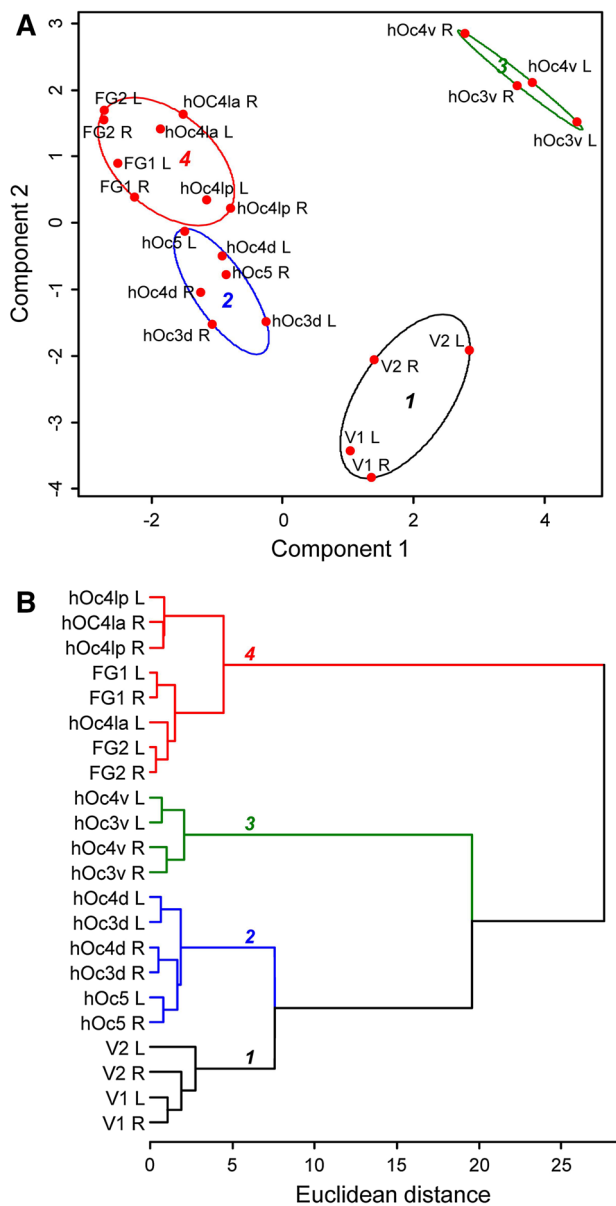


Fig. 11 Principal component (a) and hierarchical cluster (b) analyses of cytoarchitectonically defined visual areas in the human brain. The feature vectors of GLI profiles of each area and hemisphere were calculated in ten brains (see “Materials and methods”) and used for both analyses. The number of clusters was defined by Silhouette analysis. hOc4la and hOc4lp cluster together with the hierarchically high fusiform areas FG1 and FG2 and differ from the other visual areas. *L* left hemisphere, *R* right hemisphere

Continuous probabilistic cytoarchitectonic maps and stereotaxic location of areas hOc4la and hOc4lp

Continuous probabilistic cytoarchitectonic maps in the anatomical MNI reference space were calculated for areas hOc4la and hOc4lp (Fig. 12). These maps show the inter-individual variability color coded in a spectral sequence from dark blue (lowest areal presentation) to dark red

(highest areal presentation). Regions of highest overlap of all 10 examined brains are found for both areas, as well as a considerable inter-individual variability in their extent.

The centers of gravity of area hOc4la based on probability maps are $-46, -84, 3$ (left hemisphere) and $47, -81, 4$ (right hemisphere). The centers of gravity of area hOc4lp are $-35, -95, 10$ (left hemisphere) and $36, -93, 8$ (right hemisphere). Both areas are located slightly more rostrally in the right than in the left hemisphere (Table 2).

Functional properties of areas hOc4la and hOc4lp

When searching the BrainMap database for experiments activating area hOc4la, we found a total of 655 experiments (involving a total of 8760 subjects) that featured at least one focus of activation in the MPM representation of this area. 593 experiments (involving a total of 7903 subjects) were found to activate area hOc4lp.

Quantitative functional decoding based on the BrainMap meta-data reveals that both areas are involved in visual perception, in particular the processing of shapes. They are additionally activated during action observation, spatial processing, and the processing of orthography (in particular hOc4lp).

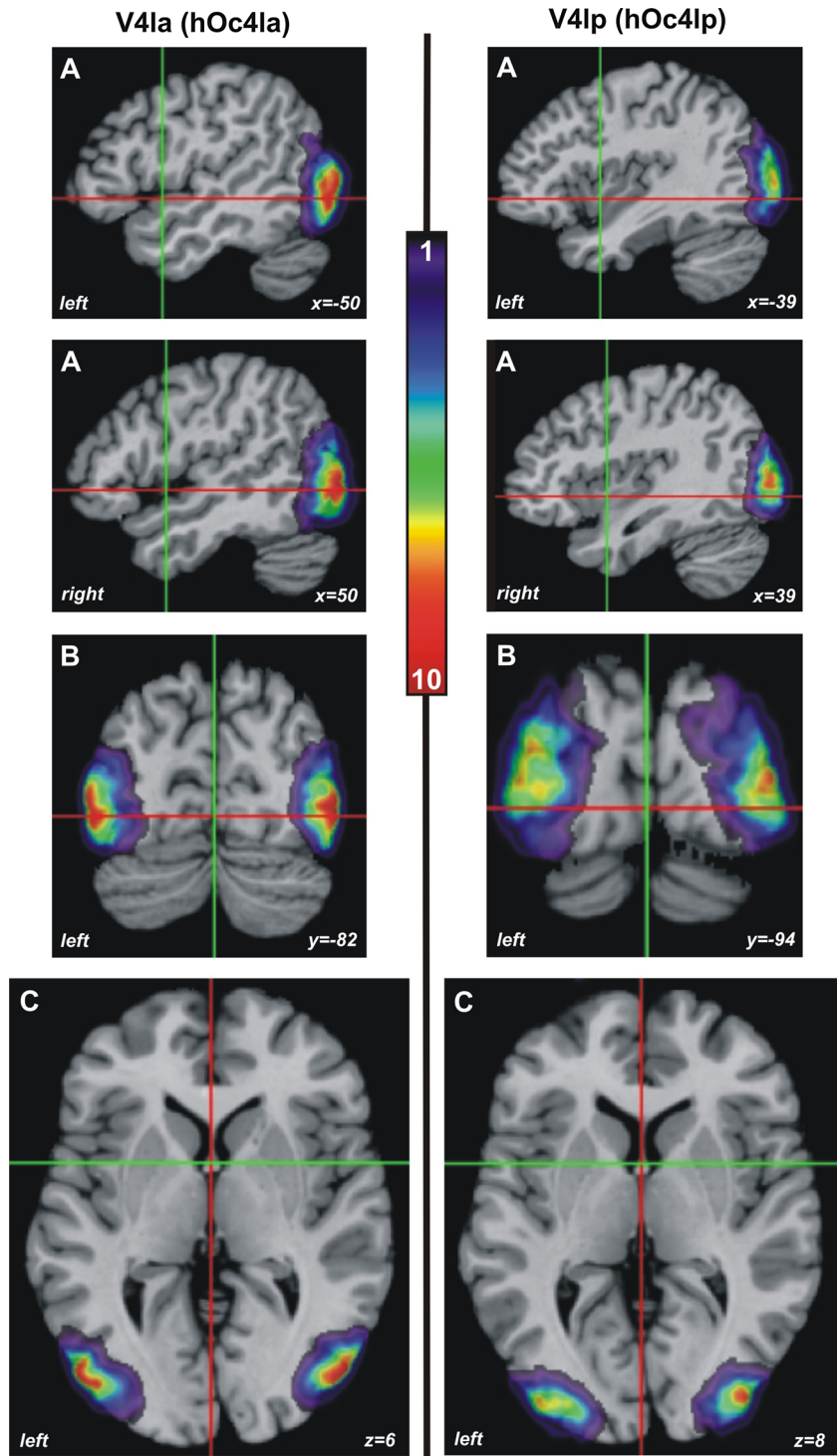
Paradigm-specific analysis showed that hOc4la and hOc4lp are activated during passive viewing, spatial location discrimination, mental rotation and subjective emotional picture discrimination. Both areas are also associated with visual attention and visual tracking. Notably, hOc4la is more strongly associated with more “receptive” functions, i.e., passive viewing paradigms such as film viewing, while hOc4lp is more strongly associated with cognitive tasks including counting and the Wisconsin card sorting test as well as language-related tasks, in particular word generation.

Functional connectivity of areas hOc4la and hOc4lp

The conjunction analysis demonstrated that overlapping co-activations of hOc4la and hOc4lp occur in visual perception of objects and faces, object recognition and object manipulation. In both hemispheres, hOc4la and hOc4lp are co-activated bilaterally with the posterior fusiform cortex (area FG2, Caspers et al. 2013), posterior parietal cortex, medial premotor cortex (SMA) and primary motor cortex (Fig. 13a–c).

Differences in functional connectivity of hOc4la and hOc4lp were assessed by computing the contrast between the two MACM maps. This analysis reveals differential co-activation likelihoods in particular for the posterior parietal cortex. In both hemispheres, hOc4la was significantly stronger connected with the superficially exposed posterior superior parietal cortex (cytoarchitectonic areas 7A and 7P;

Fig. 12 Continuous probabilistic maps of areas hOc4la and hOc4lp based on delineations in histological sections of 10 post-mortem brains in anatomical MNI space. The *color-coded map* shows the degree of overlap of the same area delineated in ten brains in a spectral sequence from *dark blue* (the area of only one brain contributes to the voxel) to *dark red* (overlap of all 10 brains). Sagittal (**a**), coronal (**b**), and horizontal (**c**) planes



Scheperjans et al. 2008) of both hemispheres. Contrastingly, hOc4lp of both hemispheres shows stronger bilateral connectivity with areas hIP1 (Choi et al. 2006) and hIP3 (Scheperjans et al. 2008) of the intraparietal sulcus (Fig. 13d).

Co-activation of hOc4la and hOc4lp occurs in areas frequently associated with language processing. hOc4la is

co-activated bilaterally with the caudal portion of the middle temporal cortex and the anterior insular cortex (Fig. 13a). Only the left hOc4la is co-activated with the inferior parietal cortex (supramarginal and angular gyri) and Broca's region of both hemispheres, whereas hOc4lp of both hemispheres is co-activated with the inferior parietal cortex (supramarginal and angular gyri), Broca's

Table 2 Coordinates of centers of gravity of the lateral occipital areas hOc4la and hOc4lp, based on probability maps after normalization in anatomical MNI space

Area	Left hemisphere			Right hemisphere		
	x	y	z	x	y	z
hOc4la	-46 ± 3.0	-84 ± 3.3	-3 ± 4.0	47 ± 1.9	-81 ± 3.5	-4 ± 5.0
hOc4lp	-35 ± 2.5	-95 ± 2.5	10 ± 7.9	36 ± 2.9	-93 ± 3.0	8 ± 6.7

Mean values (±standard deviation, SD) for the left and right hemispheres based on cytoarchitectonic mapping in ten post-mortem brains

region and anterior insular cortex of both hemispheres (Fig. 13b). Contrast analysis demonstrates that functional connectivity with Broca's region is significantly stronger for hOc4lp than hOc4la (Fig. 13d).

Discussion

Correlations with previous cytoarchitectonic maps

Area hOc4la shares a common border with the previously identified area hOc5 (Malikovic et al. 2007). The cytoarchitecture of hOc4la corresponds to that of a previously mentioned (Malikovic et al. 2007), but not delineated area located ventrally to hOc5. Here, we could define the whole extent of that area and identified it as area hOc4la. It surrounds caudal and ventral parts of area hOc5 in most cases.

Our cytoarchitectonic description of hOc4la matches in many aspects that of the area 37ac defined by Sarkisov et al. (1949). Area 37ac has a higher cell-packing density of granular layers II and IV compared to neighboring occipital areas, and layer IV borders layers III and V “in a zigzag way”, which agrees well with our finding of irregular cellular columns in layer IV, that penetrate into adjacent layers III and V. Furthermore, areas 37ac and hOc4la have a lower cell-packing density of layer V compared to layer VI and larger cells in layer V than in layer VI. hOc4la is found at a comparable location as area 37ac, i.e., in the most anterior part of the lateral occipital cortex reaching the temporo-occipital junction. However, hOc4la has a smaller dorsal extent compared to area 37ac, which occupies the most anterior parts of all three lateral occipital gyri where it extends from the inferolateral margin of the occipital lobe to the angular gyrus of the inferior parietal lobule. hOc4la is restricted to the middle and inferior lateral occipital gyri.

Ventral to the anterior part of hOc4la, we found an area that extended further into the inferior temporal cortex (Fig. 7b). The cytoarchitectonic features of this area correspond in part to area 37a defined by Sarkisov et al. (1949). It is characterized by a wide layer II, brighter sublayer IIIb (indicating either lower cell-packing density

or smaller cells), and darker sublayer IIIc (due to the presence of larger pyramidal cells). This area is located along the lateral half of the posterior fusiform gyrus and has recently been identified by Caspers et al. (2013) as area FG2. hOc4la has a lower cell-packing density compared to area FG2, particularly in layers II and IV.

The cytoarchitecture of hOc4lp fits to the description of area 19 (area praecoccipitalis) by Sarkisov et al. (1949). They found “the dominance” of layers II, III and IV compared to layers V and VI, which are reduced in their thickness, a less obvious transition between layers II and III, a well established layer III with clear transitions between its sublayers, larger pyramidal cells in sublayer IIIc, “brighter layer V” (lower in cell-packing density) with smaller cells compared to “darker layer VI” (higher in cell-packing density). All these features are found in hOc4lp. Unfortunately, Sarkisov et al. (1949) did not map regional cytoarchitectonic variations within area 19, with the exception of its dorsal part, subarea praecoccipitalis superior, which partly correlates to hOc4d (Kujovic et al. 2013). The architectonic characterization of the border between hOc4la and hOc4lp matches with that between areas 37ac and 19.

Area hOc4lp shares common borders with the previously identified dorsal extrastriate areas hOc3d and hOc4d (Kujovic et al. 2013). The border between areas hOc4lp and hOc4d is smaller compared to that between areas hOc4lp and hOc3d. The cytoarchitectonic criteria for the delineation between hOc4lp and hOc4d match our previous findings (Kujovic et al. 2013), where we described the lateral border of hOc4d. Similarly, there is an agreement between the criteria for the delineation of hOc4lp from the previously defined area hOc3d. The sizes of pyramidal cells in sublayers IIIb, IIIc and Va, as well as the cell-packing density in layers V and VI, are the most reliable criteria to differentiate hOc4lp from neighboring hOc3d (Fig. 8a).

Two extrastriate areas, hOc3v and hOc4v (Rottschy et al. 2007) are identified ventral to area hOc4lp. These areas are mainly located along the ventral surface of the occipital lobe, and occupy parts of the lateral occipital surface closer to the occipital pole. When we compare

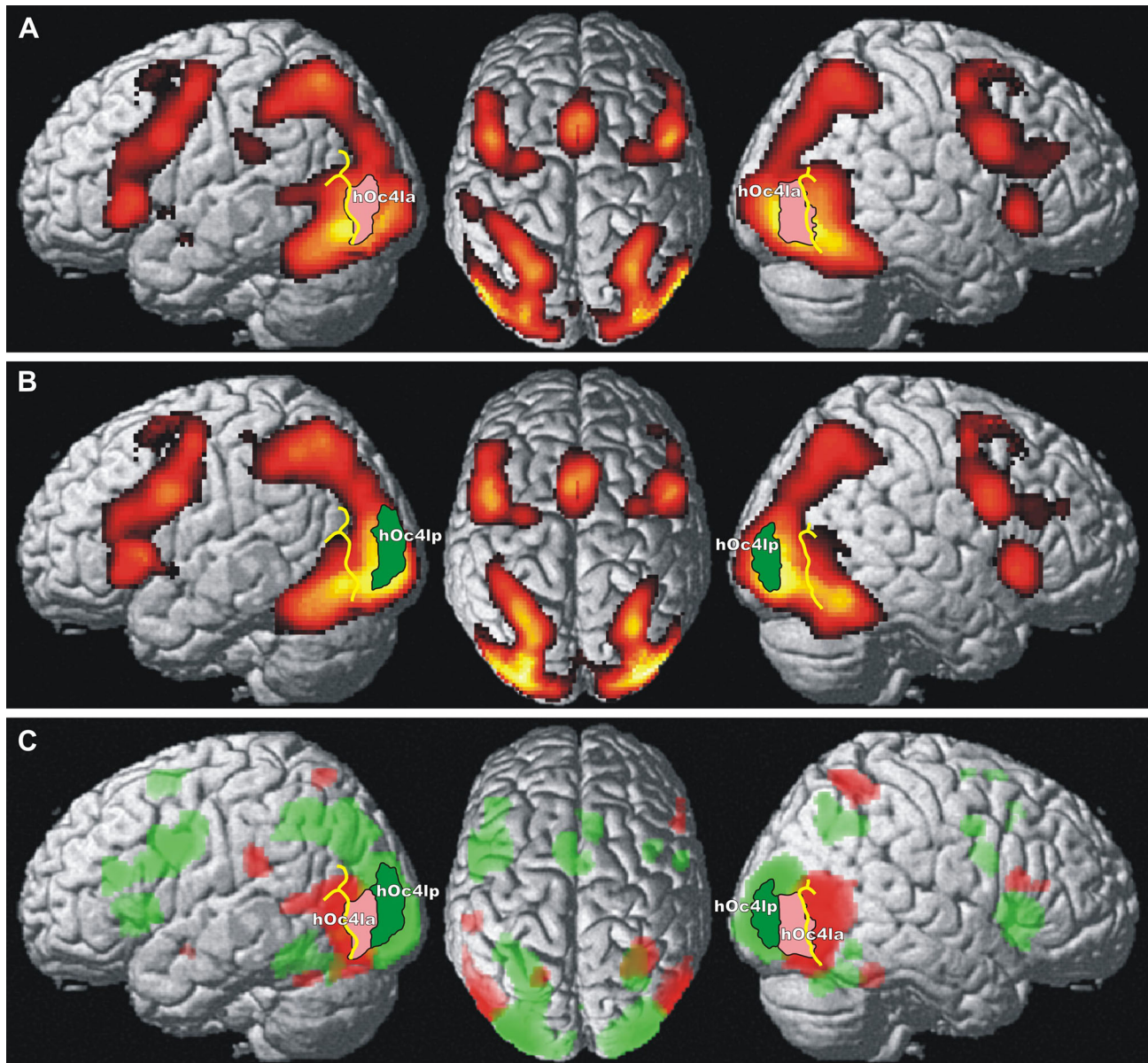


Fig. 13 Functional connectivity of the seed regions representing areas hOc4la (a) and hOc4lp (b) delineated by the significant co-activation patterns obtained in the coordinate-based meta-analysis. The color scale ranging from *deep red* (low) to *yellow* (high) indicates the strength of the effects (*z*-scores of the statistical analysis; all indicated voxels were significantly co-activated at $p < 0.05$, cluster-level corrected). The seed regions hOc4la and hOc4lp have been

delineated in the corresponding panels and color coded in *pink* (hOc4la) and *green* (hOc4lp). c The conjunction shows significant overlapping co-activations of the seed regions. d Regions showing significant differences in functional connectivity between the seed regions. Red regions code for preferential functional connectivity with hOc4la, and green regions code for preferential functional connectivity with hOc4lp). All data presented at $p < 0.05$, corrected

cytoarchitectonic description of “the cortex lateral to hOc4v” presented by Rottschy et al. (2007) with those related to our lateral occipital areas, this previously not delineated area corresponds to our hOc4lp. Rottschy et al. (2007) observed a less conspicuous transition between layers II and III, thinner and less cell dense layer IV, cell sparse layer V and clear border between layers V and VI. This is in good agreement with the present findings in hOc4lp.

The principal component analysis demonstrates that the observer-independent approach enables a quantitatively based parcellation which clearly separates different cytoarchitectonic areas. Notably, the very early visual areas V1 and V2 and the ventral stream areas hOc3v and hOc4v form two separate clusters which are located far from each other and from the other two clusters comprising the dorsal stream areas hOc3d and hOc4d as well as hOc5, and the fusiform areas FG1 and FG2 as well as areas hOc4la and

hOc4lp, respectively. The hierarchical cluster analysis supports these findings and highlights the position of hOc4la and hOc4lp at a high hierarchical level.

The sizes of hOc4la and hOc4lp did not show significant gender differences, or correlations with age. The lack of differences may be a result of the relatively small sample size for questions of this type.

Correlations to the existing human functional imaging maps

The cytoarchitectonically defined areas hOc4la and hOc4lp may correspond by their location, topographical relation to other visual areas, and coordinate-based meta-analysis to the functionally defined areas LO-2 and LO-1, respectively (Larsson and Heeger 2006). Therefore, they would be part of the object-selective lateral occipital complex.

A comparison of the sizes of LO-1 and LO-2 and hOc4la and hOc4lp with the primary visual cortex also supports the notion of a possible comparability. The surface areas of LO-1 and LO-2 are similar in size (about 331 mm²; LO-1 321(left) and 340 (right) mm² and LO-2 289 (left) and 374 (right) mm²; Larsson and Heeger 2006). Notably, the same relation was found for our volumetric data of hOc4la (2.42 cm³ in the left and 2.81 cm³ in the right hemisphere) and hOc4lp (2.64 cm³ in the left and 2.13 cm³ in the right hemisphere). Moreover, the mean surface areas of LO-1 and LO-2 occupy approximately 30 % of the mean surface area of V1 (Larsson and Heeger 2006), and the mean volumes of hOc4la and hOc4lp also amount to approximately 30 % (hOc4la is 34 % and hOc4lp is 31 %) of the mean volume of hOc1 (BA17 or V1; Amunts et al. 2007). Therefore, we think that this comparison between the functionally defined LO-1 and LO-2 (Larsson and Heeger 2006) and the cytoarchitectonically defined areas hOc4la and hOc4lp of the present observations support a good comparability.

LO-2 of Larsson and Heeger (2006) has a close topographical relationship with functionally defined areas V5/MT+ located anteriorly, and hV4 located inferiorly. This is in accordance with the present cytoarchitectonic findings, where hOc4la has comparable relationships with areas hOc5 and hOc4v (Malikovic et al. 2007; Rottschy et al. 2007). This is also found in various functional maps (e.g., Abdollahi et al. 2014). Area LO-1 is located anterior to the functionally defined area V3 and ventral to V3A. Similarly, hOc4lp shares common borders with two cytoarchitectonic areas, namely hOc3d and hOc4d (Kujovic et al. 2013), along its posterior and dorsal parts, respectively. hOc3d occupies posterior locations to hOc4d. Ventrally, LO-1 abuts cytoarchitectonic areas hOc3v and hOc4v, which overlap with functional areas V3 and hV4, VO1 or phPITv, respectively (Abdollahi et al. 2014).

Functional properties and connectivity of areas hOc4la and hOc4lp

Areas hOc4la and hOc4lp are associated with visual perception, and in particular with processing of object shape, but not with visual motion perception as shown in the present observations by quantitative functional decoding based on the BrainMap database. This is in agreement with results of Larsson and Heeger (2006), who demonstrated that areas LO-1 and LO-2 strongly responded to images of objects but were not motion selective. This object-related activity and co-activation with the posterior fusiform cortex (also an object-selective region) provide converging evidence that areas hOc4la and hOc4lp can be considered as a portion of the functionally defined LOC (Grill-Spector 2003). Furthermore, the object-related activity is important for the detection of similar shapes such as letters, and may explain involvement of hOc4la and hOc4lp in orthography and understanding of written words. Additionally, the connectivity with the posterior fusiform cortex (visual word form area FG2 of Caspers et al. 2013), middle temporal and inferior parietal cortex as well as Broca's region and the anterior insula supports involvement of these extrastriate areas in language-related processing and reading. In this context, we observed a functional segregation among areas hOc4la and hOc4lp. The contrast analysis demonstrates stronger co-activations of hOc4la with the bilateral middle temporal cortex, whereas hOc4lp shows stronger bilateral co-activation with the inferior parietal cortex and Broca's region.

Somewhat unexpected is the finding that hOc4la and hOc4lp are also significantly associated with tasks involving spatial location discrimination, mental rotation, visual attention and visual tracking. Moreover, co-activations of hOc4la and hOc4lp with the posterior parietal cortex (superior parietal and intraparietal cortex) and the premotor cortex are found here. These functional interactions suggest that both lateral occipital areas are also potentially involved in a functional network related to spatial- and action-related processing. Furthermore, supplementary contrast analyses showed that hOc4la is more closely connected with the superior parietal cortex compared to hOc4lp, which shows significantly stronger functional connectivity with the intraparietal cortex (Fig. 13d). These findings further support the above mentioned functional segregation among the two cytoarchitectonic areas.

Our functional and connectivity data of hOc4la and hOc4lp suggest that these extrastriate areas may interact with both the dorsal and ventral visual processing streams, rather than exclusively participate in one of these two streams (see Larsson and Heeger 2006). Our findings further suggest that the cytoarchitectonically (hOc4la and hOc4lp) and functionally (LO-2 and LO-1) defined areas in

the region of the lateral occipital cortex may be considered comparable. Finally, these two extrastriate areas seem to represent the anatomical equivalent to the lateral occipital complex (LO; divided into LO-1 and LO-2, Weiner and Grill-Spector 2011), an area involved in the visual object recognition originally described by Malach et al. (1995), which is located immediately behind area V5/MT+.

Acknowledgments The research leading to these results was partly funded by the European Union Seventh Framework Programme (FP7/2007–2013) under grant agreement No. 604102 (Human Brain Project). The authors thank Mrs. Ursula Blohm and Ms. Ferdag Kocaer for excellent histological assistance, and Dr. Sebastian Bludau for technical support.

References

- Abdollahi RO, Kolster H, Glasser MF, Robinson EC, Coalson TS, Dierker D, Jenkinson M, van Essen DC, Orban GA (2014) Correspondences between retinotopic areas and myelin maps in human visual cortex. *Neuroimage* 99:509–524
- Amunts K, Zilles K (2001) Advances in cytoarchitectonic mapping of the human cerebral cortex. *Neuroimaging Clin N Am* 11:151–169
- Amunts K, Malikovic A, Mohlberg H, Schormann T, Zilles K (2000) Brodmann's areas 17 and 18 brought into stereotaxic space—where and how variable? *Neuroimage* 11:66–84
- Amunts K, Weis PH, Mohlberg H, Pieperhoff P, Gurd J, Shah JN, Marshall CJ, Fink GR, Zilles K (2004) Analysis of the neural mechanisms underlying verbal fluency in cytoarchitectonically defined stereotaxic space—the role of Brodmann's areas 44 and 45. *Neuroimage* 22:42–56
- Amunts K, Kedo O, Kindler M, Pieperhoff P, Schneider F, Mohlberg H, Habel U, Shah JN, Zilles K (2005) Cytoarchitectonic mapping of the human amygdale, hippocampal region and entorhinal cortex. *Anat Embryol* 210:343–352
- Amunts K, Armstrong E, Malikovic A, Hörmke L, Mohlberg H, Schleicher A, Zilles K (2007) Gender-specific left-right asymmetries in human visual cortex. *J Neurosci* 27(6):1356–1364
- Bartels P (1979) Numerical evaluation of cytologic data. II. Comparison of profiles. *Anal Quant Cytol* 1:77–83
- Caspers S, Geyer S, Schleicher A, Mohlberg H, Amunts K, Zilles K (2006) The human inferior parietal cortex: cytoarchitectonic parcellation and interindividual variability. *Neuroimage* 33:430–448
- Caspers S, Zilles K, Eickhoff SB, Schleicher A, Mohlberg H, Amunts K (2013) Cytoarchitectonical analysis and probabilistic mapping of two extrastriate areas of the human posterior fusiform gyrus. *Brain Struct Funct* 218(2):511–526
- Choi H-J, Zilles K, Mohlberg H, Schleicher A, Fink G, Armstrong E, Amunts K (2006) Cytoarchitectonic identification and probabilistic mapping of two distinct areas within the anterior ventral bank of the human intraparietal sulcus. *J Comp Neurol* 495(1):53–69
- Cieslik EC, Zilles K, Caspers S, Roski C, Kellermann TS, Jakobs O, Langner R, Laird AR, Fox PT, Eickhoff S (2013) Is there “One” DLPFC in cognitive action control? Evidence for heterogeneity from co-activation-based parcellation. *Cereb Cortex* 23(11):2677–2689
- Collins DL, Neelin P, Peters TM, Evans AC (1994) Automatic 3D intersubject registration of MR volumetric data in standardized Talairach space. *J Comput Assist Tomogr* 18:192–205
- Dupont P, De Bruyn B, Vandenberghe R, Rosier AM, Michiels J, Marchal G, Mortelmans L, Orban GA (1997) The kinetic occipital region in human visual cortex. *Cereb Cortex* 7:283–292
- Eickhoff SB, Stephan KE, Mohlberg H, Grefkes C, Fink GR, Amunts K, Zilles K (2005) A new SPM toolbox for combining probabilistic cytoarchitectonic maps and functional imaging data. *Neuroimage* 25:1325–1335
- Eickhoff SB, Paus T, Caspers S, Grosbras MH, Evans AC, Zilles K, Amunts K (2007) Assignment of functional activations to probabilistic cytoarchitectonic areas revisited. *Neuroimage* 36:511–521
- Eickhoff SB, Laird AR, Grefkes C, Wang LE, Zilles K, Fox PT (2009) Coordinate-based activation likelihood estimation meta-analysis of neuroimaging data: a random-effects approach based on empirical estimates of spatial uncertainty. *Hum Brain Mapp* 30(9):2907–2926
- Eickhoff SB, Bzdok D, Laird AR, Caspers S, Zilles K, Fox PT (2011) Co-activation patterns distinguish cortical modules their connectivity and functional differentiation. *Neuroimage* 57(3):938–949
- Eickhoff SB, Bzdok D, Laird AR, Kurth F, Fox PT (2012) Activation likelihood estimation meta-analysis revisited. *Neuroimage* 59(3):2349–2361
- Evans AC, Collins DL, Mills SR, Brown ED, Kelly RL, Peters TM (1993) 3D statistical neuroanatomical models from 305 MRI volumes. In: Proceeding of the IEEE-NSS-MI Symposium London. MTP press, UK, pp 1813–1817
- Glasser MF, van Essen DC (2011) Mapping human cortical areas in vivo based on myelin content as revealed by T1- and T2-weighted MRI. *J Neurosci* 31:11597–11616
- Glasser MF, Goyal MS, Preuss TM, Raichle ME, van Essen DC (2014) Trends and properties of human cerebral cortex: correlations with cortical myelin content. *Neuroimage* 93:165–175
- Goldman PS, Nauta WJH (1977) Columnar distribution of cortico-cortical fibers in the frontal association, limbic, and motor cortex of the developing rhesus monkey. *Brain Res* 122:393–413
- Goldman-Rakic PS (1984) Modular organization of prefrontal cortex. *TINS* 7:419–429
- Goldman-Rakic PS (1995) Anatomical and functional circuits in prefrontal cortex of nonhuman primates. In: Jasper HH, Riggio S, Goldman-Rakic PS (eds) *Epilepsy and the Functional Anatomy of the Frontal Lobe*. Raven Press, New York, pp 51–65
- Goldman-Rakic PS, Schwartz ML (1982) Interdigitation of contralateral and ipsilateral columnar projections to frontal association cortex in primates. *Science* 216:755–757
- Grill-Spector K (2003) The neural basis of object perception. *Curr Opin Neurobiol* 13(2):159–166
- Grill-Spector K, Kushnir T, Edelman S, Avidan G, Itzhak J, Malach R (1999) Differential processing of objects under various viewing conditions in the human lateral occipital complex. *Neuron* 24:187–203
- Grill-Spector K, Kourtzi Z, Kanwisher N (2001) The lateral occipital complex and its role in object recognition. *Vision Res* 41:1409–1422
- Grossman E, Donnelly M, Price R, Pickens D, Morgan V, Neighbor G, Blake R (2000) Brain areas involved in perception of biological motion. *J Cogn Neurosci* 12(5):711–720
- Henn S, Schormann T, Engler K, Zilles K, Witsch K (1997) Elastische Anpassung in der digitalen Bildverarbeitung auf mehreren Auflösungsstufen mit Hilfe von Mehrgitterverfahren. In: Paulus E, Wahl FM (eds) *Mustererkennung 1997*. Springer, Berlin, pp 392–399
- Henriksson L, Karvonen J, Salminen-Vaparanta N, Railo H, Vanni S (2012) Retinotopic maps, spatial tuning, and locations of human visual areas in surface coordinates characterized with multifocal and blocked fMRI designs. *PLoS One* 7(5):e36859

- Holmes CJ, Hoge R, Collins L, Woods R, Toga AW, Evans AC (1998) Enhancement of MR images using registration for signal averaging. *J Comput Assisted Tomogr* 22:324–333
- Hömké L (2006) A multigrid method for anisotropic PDE's in elastic image registration. *Numer Linear Algebra Appl* 13:215–229
- Jones SE, Buchbinder BR, Aharon I (2000) Three-dimensional mapping of cortical thickness using laplace's equation. *Hum Brain Mapp* 11:12–32
- Kellermann TS, Caspers S, Fox PT, Zilles K, Roski C, Laird AR, Turetsky BI, Eickhoff SB (2013) Task- and resting-state functional connectivity of brain regions related to affection and susceptible to concurrent cognitive demand. *Neuroimage* 72:69–82
- Kolster H, Peeters R, Orban GA (2010) The retinotopic organization of the human middle temporal area MT/V5 and its cortical neighbors. *J Neurosci* 30(29):9801–9820
- Kononen M, Paakkonen A, Pihlajamaki M, Partanen K, Karjalainen PA, Soimakallio S, Aronen HJ (2003) Visual processing of coherent rotation in the central visual field: an fMRI study. *Perception* 32(10):1247–1257
- Kourtzi Z, Kanwisher N (2001) Representation of perceived object shape by the human lateral occipital complex. *Science* 293:1506–1509
- Kourtzi Z, Erb M, Grodd W, Bülthoff H (2003) Representation of the perceived 3-D object shape in the human lateral occipital complex. *Cereb Cortex* 13(9):911–920
- Kujovic M, Zilles K, Malikovic A, Schleicher A, Rottschy C, Mohlberg H, Eickhoff S, Amunts K (2013) Cytoarchitectonic mapping of the dorsal extrastriate human visual cortex. *Brain Struct Funct* 2018(1):157–172
- Laird AR, Eickhoff SB, Kurth F, Fox PM, Uecker AM, Turner JA, Robinson JL, Lancaster JL, Fox PT (2009) ALE meta-analysis workflows via the BrainMap database: progress towards a probabilistic functional brain atlas. *Front Neuroinform* 3:23
- Laird AR, Eickhoff SB, Fox PM, Uecker AM, Ray KL, Saenz JJ Jr, McKay DR, Bzdok D, Laird RW, Robinson JL, Turner JA, Turkeltaub PE, Lancaster JL, Fox PT (2011) The BrainMap strategy for standardization, sharing, and meta-analysis of neuroimaging data. *BMC Res Notes* 4(349):349
- Larsson J, Heeger DJ (2006) Two retinotopic visual areas in human lateral occipital cortex. *J Neurosci* 26(51):13128–13142
- Larsson J, Heeger DJ, Landy MS (2010) Orientation selectivity of motion-boundary responses in human visual cortex. *J Neurophysiol* 104(6):2940–2950
- Mahalanobis PC, Majumda DN, Rao DC (1949) Anthropometric survey of the united provinces. A statistical study. *Sankhya* 9:89–324
- Malach R, Reppas JB, Benson RR, Kwong KK, Jiang H, Kennedy WA, Ledden PJ, Brady TJ, Rosen BR, Tootell RBH (1995) Object-related activity revealed by functional magnetic resonance imaging in human occipital cortex. *Proc Natl Acad Sci* 92:8135–8139
- Malikovic A, Amunts K, Schleicher A, Mohlberg H, Eickhoff SB, Wilms M, Palomero-Gallagher N, Armstrong E, Zilles K (2007) Cytoarchitectonic analysis of the human extrastriate cortex in the region V5/MT+: a probabilistic, stereotaxic map of area hOc5. *Cereb Cortex* 17(3):562–574
- Malikovic A, Vučetić B, Milisavljević M, Tosevski J, Sazdanović P, Milojević B, Malobabić S (2012) Occipital sulci of the human brain: variability and morphometry. *Anat Sci Int* 87(2):61–70
- Merker B (1983) Silver staining of cell bodies means of physical development. *J Neurosci Methods* 9:235–241
- Murray SO, Olshausen BA, Woods DL (2003) Processing shape, motion and three-dimensional shape-from-motion in the human cortex. *Cereb Cortex* 13(5):508–516
- Press WA, Brewer AA, Dougherty RF, Wade AR, Wandell BA (2001) Visual areas and spatial summation in human visual cortex. *Vision Res* 41:1321–1332
- Reetz K, Dogan I, Rolfs A, Binkofski F, Schulz JB, Laird AR, Fox PT, Eickhoff SB (2012) Investigating function and connectivity of morphometric findings-exemplified on cerebellar atrophy in spinocerebellar atrophy 17 (SCA17). *Neuroimage* 62(3):1354–1366
- Rottschy C, Eickhoff SB, Schleicher A, Mohlberg H, Kujovic M, Zilles K, Amunts K (2007) Ventral visual cortex in humans: cytoarchitectonic mapping of two extrastriate areas. *Hum Brain Mapp* 28:1045–1059
- Rottschy C, Caspers S, Roski C, Reetz K, Dogan I, Schulz JB, Zilles K, Laird AR, Fox PT, Eickhoff SB (2012) Differentiated parietal connectivity of frontal regions for “what” and “where” memory. *Brain Struct Funct* 218(6):1551–1567
- Sarkheil P, Vuong QC, Bülthoff HH, Noppeney U (2008) The integration of higher order form and motion by the human brain. *Neuroimage* 42:1529–1536
- Sarkisov SA, Filimonoff IN, Preobrazhenskaya NS (1949) Cytoarchitecture of the human cortex cerebri. Medgiz, Moscow, Russia (in Russian)
- Sawamura H, Georgieva S, Vogels R, Vanduffel W, Orban GA (2005) Using functional magnetic resonance imaging to assess adaptation and size invariance of shape processing by humans and monkeys. *J Neurosci* 25(17):4294–4306
- Sayres R, Grill-Spector K (2008) Relating retinotopic and object-selective responses in human lateral occipital cortex. *J Neurophysiol* 100:249–267
- Schepers F, Eickhoff SB, Hömké L, Mohlberg H, Hermann K, Amunts K, Zilles K (2008) Probabilistic maps, morphometry, and variability of cytoarchitectonic areas in human superior parietal cortex. *Cereb Cortex* 18(9):2141–2157
- Schleicher A, Zilles K (1990) A quantitative approach to cytoarchitectonics: analysis of structural inhomogeneities in nervous tissue using an image analyser. *J Microsc* 157:367–381
- Schleicher A, Palomero-Gallagher N, Morosan P, Zilles K (1999) Observer-independent method for microstructural parcellation of cerebral cortex: a quantitative approach to cytoarchitectonics. *Neuroimage* 9:165–177
- Schleicher A, Amunts K, Geyer S, Kowalski T, Schormann T, Palomero-Gallagher N, Zilles K (2000) A stereological approach to human cortical architecture: identification and delineation of cortical areas. *J Chem Neuroanat* 20:31–47
- Schleicher A, Palomero-Gallagher N, Morosan P, Eickhoff SB, Kowalski T, de Vos K, Amunts K, Zilles K (2005) Quantitative architectural analysis: a new approach to cortical mapping. *Anat Embryol* 210(5–6):373–386
- Schmitt O, Böhme M (2002) A robust transcranial profile scanner for generating 2-d traverses in histological sections of richly curved cortical courses. *Neuroimage* 16:1103–1119
- Seiffert AE, Somers DC, Dale AM, Tootell RBH (2003) Functional MRI studies of human visual motion perception: texture, luminance, attention and after-effects. *Cereb Cortex* 13(4):340–349
- Sereno MI, Dale AM, Reppas JB, Kwong KK, Belliveau JW, Brady TJ, Rosen BR, Tootell RB (1995) Borders of multiple visual areas in humans revealed by functional magnetic resonance imaging. *Science* 268:889–893
- Smith AT, Greenlee MW, Singh KD, Kraemer FM, Hennig J (1998) The processing of first- and second-order motion in human visual cortex assessed by functional magnetic resonance imaging (fMRI). *J Neurosci* 18:3816–3830
- Stanley D, Rubin N (2005) Rapid detection of salient regions: evidence from apparent motion. *J Vis* 5:690–701

- Swisher JD, Halko MA, Merabet LB, McMains SA, Somers DC (2007) Visual topography of human intraparietal sulcus. *J Neurosci* 27(20):5326–5337
- Talairach J, Tournoux P (1988) Coplanar stereotaxic atlas of the human brain. Thieme, Stuttgart
- Tootell RB, Hadjikhani N (2001) Where is ‘dorsal V4’ in human visual cortex? Retinotopic, topographic and functional evidence. *Cereb Cortex* 11:298–311
- Van Oostende S, Sunaert S, Van Hecke P, Marchal G, Orban GA (1997) The kinetic occipital (KO) region in man: an fMRI study. *Cereb Cortex* 7(7):690–701
- Vinberg J, Grill-Spector K (2008) Representation of shapes, edges and surfaces across multiple cues in the human visual cortex. *J Neurophysiol* 99:1380–1393
- Wandell BA, Dumoulin SO, Brewer AA (2007) Visual field maps in human cortex. *Neuron* 56:366–383
- Weiner KS, Grill-Spector K (2011) Not one extrastriate body area: using anatomical landmarks, hMT+, and visual field maps to parcellate limb-selective activations in human lateral occipitotemporal cortex. *NeuroImage* 56:2183–2199
- Wree A, Schleicher A, Zilles K (1982) Estimation of volume fractions in nervous tissue with an image analyzer. *J Neurosci Methods* 6:29–43
- Zeki S, Perry RJ, Bartels A (2003) The processing of kinetic contours in the brain. *Cereb Cortex* 13(2):189–202
- Zilles K, Schleicher A, Palomero-Gallagher N, Amunts K (2002) Quantitative analysis of cyto- and receptor architecture of the human brain. In: Mazziota J, Toga A (eds) Brain Mapping: the methods, 2nd edn. Academic Press, New York, pp 573–602